Summer 2011

Non-homogeneous Hybrid Rocket Fuel for Enhanced Regression Rates Utilizing Partial Entrainment

Kenny Michael Boronowsky
San Jose State University

NON-HOMOGENEOUS HYBRID ROCKET FUEL FOR ENHANCED REGRESSION RATES UTILIZING PARTIAL ENTRAINMENT

A Thesis

Presented to

The Faculty of the Department of Mechanical and Aerospace Engineering

San Jose State University

In Partial Fulfillment

Of the Requirements for the Degree

Master of Science

by

Kenny Boronowsky

May 2011

The Designated Thesis Committee Approves the Thesis Titled

NON-HOMOGENEOUS HYBRID ROCKET FUEL FOR ENHANCED REGRESSION RATES UTILIZING PARTIAL ENTRAINMENT

by

Kenny Boronowsky

APPROVED FOR THE DEPARTMENT OF MECHANICAL AND AEROSPACE ENGINEERING

SAN JOSÉ STATE UNIVERSITY

August 2011

Dr. Periklis Papadopoulos	Department of Mechanical and Aerospace Engineering
Dr. Nikos Mourtos	Department of Mechanical and Aerospace Engineering
Marcus Murbach	NASA Ames Research Center

ABSTRACT

NON-HOMOGENEOUS HYBRID ROCKET FUEL FOR ENHANCED REGRESSION RATES UTILIZING PARTIAL ENTRAINMENT

by Kenny Boronowsky

A concept was developed and tested to enhance the performance and regression rate of hydroxyl terminated polybutadiene (HTPB), a commonly used hybrid rocket fuel. By adding small nodules of paraffin into the HTPB fuel, a non-homogeneous mixture was created resulting in increased regression rates. The goal was to develop a fuel with a simplified single core geometry and a tailorable regression rate. The new fuel would benefit from the structural stability of HTPB yet not suffer from the large void fraction representative of typical HTPB core geometries.

Regression rates were compared between traditional HTPB single core grains, 85% HTPB mixed with 15% (by weight) paraffin cores, 70% HTPB mixed with 30% paraffin cores, and plain paraffin single core grains. Each fuel combination was tested at oxidizer flow rates, ranging from 0.9 - 3.3 g/s of gaseous oxygen, in a small scale hybrid test rocket and average regression rates were measured.

While large uncertainties were present in the experimental setup, the overall data showed that the regression rate was enhanced as paraffin concentration increased. While further testing would be required at larger scales of interest, the trends are encouraging. Inclusion of paraffin nodules in the HTPB grain may produce a greater advantage than other more noxious additives in current use. In addition, it may lead to safer rocket motors with higher integrated thrust due to the decreased void fraction.

ACKNOWLEDGEMENTS

I would like to thank the entire Aerospace Engineering faculty including Dr. Papadopoulos and Dr. Mourtos. Their support and guidance were critical in my work. I would also like to thank Marcus Murbach from NASA Ames Research Center for his dedication and tremendous support of my project in addition to his technical oversight.

A special thanks is made to my father Michael Boronowsky. None of this would have been possible without his help and support. His constant dedication of helping me build hardware, cast motors, perform tests, and bounce ideas off of was the enabling factor in the completion of this work. He hand built and designed nearly all of the electrical equipment in the motor test stand, machined many of the parts for me, and provided countless hours of help during manufacturing and testing. He spent the majority of his free time helping me with this project and was an integral part of the hundreds of tests we performed from his garage.

Table of Contents

List of Tables

List of Figures

I. INTRODUCTION

A. HISTORY AND BACKGROUND

Hybrid rockets are simply a type of rocket that utilize their fuel and oxidizer in two separate phases. They have been studied since the early 1930s but have yet to reach the same level of adoption as solid fuel rockets and liquid fuel rockets. While relatively old, research in hybrid rocketry is still a developing field with many avenues for improvement and better understanding. Many countries, universities, companies, and individuals have committed appreciable efforts into furthering this research and creating potential applications for its use. Some of these efforts have found their way into commercial vehicles such as SpaceShip One and Two as well as other sub-orbital tourism vehicles. Other similar efforts are working on putting small payloads into orbit utilizes cheap and reusable rocket stages based on current hybrid research. Many other applications have been proposed or are in development as well. With all these future applications on the horizon including manned flight, optimizations in performance and usability are going to be viable lines of research that can impact the ability for hybrid rockets to compete with more traditional systems.

A brief diagram of a hybrid motor system is shown below in Fig. I-1 to give overview of what traditional hybrid motors entail.

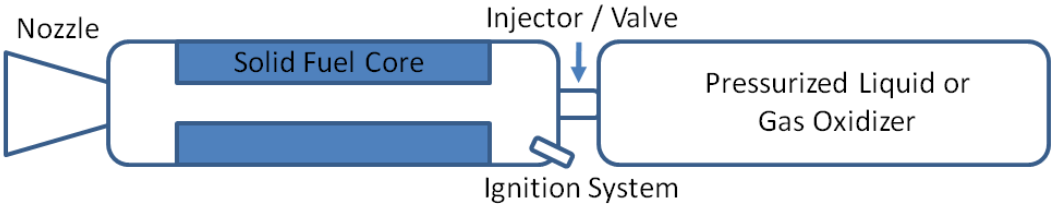

Fig. I-1 Basic Hybrid Rocket

The key feature as previously stated was that hybrid rockets utilize the fuel and oxidizer in two separate phases. This method is in contrast to liquid rockets which utilize the fuel and oxidizer both in liquid or gas form and also in contrast to solid rockets which mix oxidizer with fuel into a single solid fuel. In general there is some sort of pressurized oxidizer tank that feeds gas or liquid into the chamber that contains the solid fuel. Other variations exist with opposite phases or other more exotic combinations. A single valve and flow control unit can be used to throttle the engine by regulating the oxidizer flow rate. Oxidizer tanks can be self pressurized or pressurized by an external high pressure source. There is no turbo pump machinery such as those needed in liquid rockets. The rocket is also able to be shut down, throttle or potentially restarted which is currently not possible in solid rockets. Hybrids fall in between solid and liquid rockets in terms of complexity and performance. They do however offer substantial benefits in safety and usability over solid alternatives since the oxidizer is kept separate from the fuel.

The oxidizers that are most commonly used are liquid Oxygen (LOX) and Nitrous Oxide (N_2O). There are many other oxidizers that can be used but do to toxicity, reactivity, performance, storability and cost; these two are the most desirable. Research into other more exotic oxidizers and oxidizer combinations are an ongoing effort. In

most modern systems today, N_2O is the oxidizer of choice due to its self pressurization ability, storage density and safety. LOX systems are traditionally higher performance but require external pressurization and systems inside the engine to convert the liquid oxidizer to gas for combustion with the fuel.

In modern hybrid rockets, the traditional and most widely understood fuel is Hydroxyl Terminated Polybutadiene (HTPB). It has the consistency of a hard rubber and can be combined with modifiers for strength, burn rate and burn temperature. HTPB has been a common binder and fuel for solid rockets for many decades. It is very stable and relatively easy to cast into different fuel geometries. When burned with common oxidizers, the byproducts of the reaction are relatively safe when compared to more exotic fuels.

While burn performance is not necessarily poor for HTPB, it widely considered that HTPB regression rate is slow and not suitable for many high thrust applications. In order to overcome the low regression rate, several techniques are used to improve performance. Additives can be mixed into the HTPB during casting to marginally improve burn rate. Many of these additives can be effective but sometimes suffer from the fact that they can be toxic, expensive or increase the combustion temperature which can complicate engine design. The more common technique is to form complicated fuel core geometries to increase the surface area of the fuel that can be burned. An illustration is shown below in Fig. I-2 which highlights this complicated geometry.

Fig. I-2 HTPB fuel with "wagon wheel" geometry

These "wagon wheel" fuel core geometries are very effective in increasing the mass flux of the fuel during a burn. They also introduce a few negative side effects. The void fraction (fraction of how much empty space is wasted inside engine) is increased substantially which reduces the space efficiency of the motor and can lead to an increase in structural mass. The more prominent issue with this configuration is what happens when the fuel slivers burn down too thin. If the engine is burned too long, the fuel slivers get very thin and can break off and plug up the nozzle of the rocket. To combat this issue, the engine must be shut down early to prevent the fuel web from breaking up. This results in a larger quantity of unburned fuel left in the motor and decreases the overall efficiency of the design since the extra fuel is wasted mass.

In recent years new types of high regression rate fuels have been explored that offer better thrust, performance and simplify the fuel core geometry. One of the most promising has been the use of paraffin wax. Pioneered at Stanford University and since studied by many universities, paraffin fuel is likely to become one of the more common hybrid fuels in the future. Paraffin fuels have very low melting points and benefit during greatly from a process called entrainment where a liquid layer of fuel forms on the surface of the fuel and small droplets of fuel are pulled into or past the combustion flame and burn much more efficiently and quickly. Paraffin fuels offer a 3-4x [9] improvement

over HTPB in regression rate which allows for much higher thrusting engines due to the increase in mass flow rate of the fuel.

Other advanced concepts currently being studied regarding swirling injection and novel chamber designs are showing some initial results that can also benefit the research towards higher regression rate fuels. The hybrid rocket research field has become very diverse in concepts and methods. This paper will not cover some of these past or present experimental techniques for increasing burn rates or improving efficiency, but rather focus on a comparison of traditional burn rates vs a new combination fuel.

B. NON-HOMOGENEOUS FUEL CONCEPT

While high performance fuels like paraffin that utilize entrainment in the combustion process are currently the focus of much of the advanced research in hybrid rocket fuels, there are potential applications in which paraffin may not be the best suited. Potential applications may call for a fuel that has better thermal stability and higher structural capabilities than paraffin fuels currently offer. Research is currently being conducted into harder and higher melting point paraffins that can possibly fill more applications and scenarios where ambient heat or structural loads are greater than current paraffin based fuels can survive.

An alternative potential solution to this issue is the primary focus of this thesis paper. In particular the idea of creating a new fuel combination to enhance regression rates was under consideration. The main focus would be to create a fuel that was mainly constituted with HTPB but would yield an appreciable regression rate increase without increasing the toxicity or simplicity of casting. The rationale was that HTPB has much

better structural and thermal capabilities compared to high regression fuels and would serve many applications well if the regression rate could be increased and the fuel geometry kept to a simple single core as opposed to the "wagon wheel" geometry.

Several HTPB based fuel combinations were investigated but after testing and manufacturing trials, the main focus became mixing HTPB and paraffin. Both paraffin and HTPB burn “clean” with respect to many other fuels that can be used. They are also both very easy to obtain and easy to work with since they are non hazardous. Casting and formulation of HTPB is very well understood in the rocketry industry. Paraffin is also easy to cast and pour since it can simply be heated past its melting point and poured into a mold.

Since paraffin regression rate was significantly higher than that of pure HTPB, it was theorized that mixing paraffin into the HTPB would increase the HTPB regression rate. Mixing the two fuels homogeneously did not seem like the best approach due to the lack of knowledge of what the chemical structure of the actual mer chains would result in from the polymerization process. Instead a non-homogeneous approach was taken that would involve mixing in granulated chunks of paraffin into the HTPB during the casting and curing process. These chunks would remain intact inside the HTPB fuel core during casting. During the motor burn, the fuel would regress down to these pockets of paraffin and release small blobs of paraffin into the combustion flame similar to the process of entrainment in conventional paraffin motors. More detail on the theory behind this non-homogeneous fuel is discussed in Section II-C. Details on formulation and casting method can be seen in Section IV-D.

C. POTENTIAL BENEFITS AND APPLICATIONS

As stated earlier, the non-homogeneous fuel in development could offer some benefits in the areas that conventional paraffin motors struggle. While it is hypothesized that the non-homogeneous fuel will not have comparable performance in terms of regression rate to normal paraffin, it should offer a sizable benefit over standard HTPB. The proposed benefits of this new fuel would be as follows:

- Non toxic (In casting, handling and burning)
- Simple casting technique
- Higher regression / thrust compared to standard HTPB
- Increased structural capability compared to paraffin
- Increased resistance to melting prior to launch compared to paraffin
- Simpler fuel core geometry compared to standard HTPB with similar fuel mass flux resulting in small void fraction
- Tailorable regression rate by varying mixing concentrations of respective fuels which leads to tailorable thrust

Potential applications that were initially investigated were for sounding rocket sustainer stage replacement. Typically in a sustainer stage, a tailored thrust and thrust duration is desirable to achieve the proper altitude needed for a payload or experiment. For this application it was hypothesized that paraffin may burn too quickly and be difficult to efficiently throttle to the potentially low thrust levels that a mission could need. HTPB could throttle lower but would suffer from the large void fraction and wagon wheel geometry. Tailoring a fuel to offer the performance desired at peak

efficiency un-throttled would be ideal. The stage could be optimized for mass and performance to better match mission requirements. Having a low void fraction would also help minimize structural weight and maximize the achievable altitude. The entire system would also be less susceptible to ambient temperature extremes compared to paraffin fuels. A potential design was investigated to serve this purpose illustrated below in Fig. I-3.

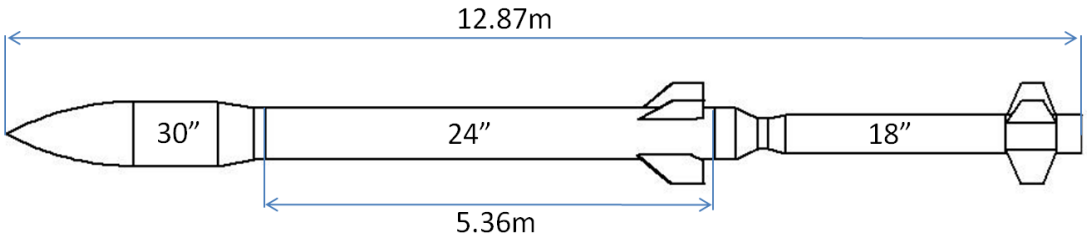

Fig. I-3 Potential hybrid sounding rocket configuration

The design shown would utilize a common booster used in the NASA sounding rocket program called the Terrier. A 24 inch hybrid section that could be recovered and reused would be on top of the booster and allow for payloads up to 30 inches. Such a configuration would be price and performance competitive to the Black Brant line of sounding rockets and, if it was made reusable, could significantly drive down the cost. The design above was carried only through initial sizing and is not covered in this paper.

II. THEORY

A. CLASSICAL REGRESSION THEORY

The classical regression theory discussed for the scope of this paper will be in the area of HTPB and other traditional solid fuels. Classical theory for hybrid fuel regression dates back to early investigations in the early 1940s. While many current models exist that try to address different physical models or mechanisms, the heat-transfer diffusion-limited theory originally developed by Marxman in the 1960s is the most common starting point for classical regression theory [12]. Accuracy of the model has increased from additions and other modifications over the years by numerous researchers for fuels such as HTPB and HTPB-blended fuels.

An overview image of classical regression in a HTPB-based hybrid model is shown in Fig. II-1. The basic and simplified physical model involves transferring heat to the solid fuel surface to the extent that pyrolization occurs at the fuel surface. The solid fuel regresses and releases gaseous fuel into the fuel-rich zone area pictured. Incoming oxidizer enters the boundary layer of the flow and mixes with the fuel. At the point where the mixture is sufficient, a combustion flame forms. This combustion flame transfers heat to the solid fuel surface through radiation and convection to enable further pyrolysis. Heat transfer through convection is generally much larger than radiation unless metal additives are mixed into the fuel [12].

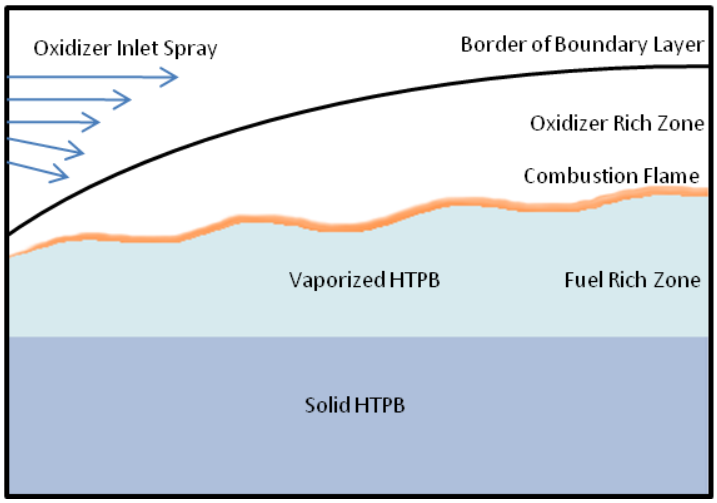

Fig. II-1 Theoretical physical model of regression for classical fuels

To illustrate the energy balance in the heat-transfer diffusion-limited model, Fig. II-2 is used [12]. The following set of equations and derivations follows the derivation by Sutton [12], which is based on Marxman's regression theory.

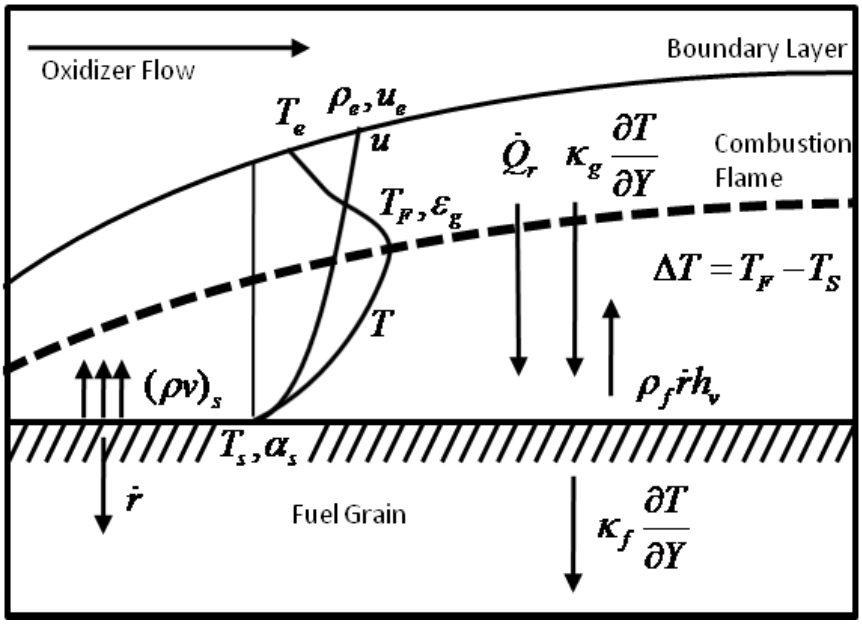

Fig. II-2 General energy balance for the heat-transfer diffusion-limited model

The general energy balance in this model can be summarized in equation 2.1.

$$Q_{convection} + Q_{radiation\ in} = Q_{conduction\ out} + Q_{phase\ change} + Q_{radiation\ out} \quad (2.1)$$

Since radiation in non-metalized fuels is typically low and solid phase heat conduction is usually small as well, they can be neglected in this simple analysis. The resulting equation 2.2 or expanded 2.3 simplifies to show that the energy transferred into the fuel by convection is equal to the multiplication of the solid fuel density, the surface regression rate, and the over-all heat of vaporization of the fuel.

$$\dot{Q}_s = \dot{Q}_c \quad (2.2)$$

Therefore:

$$\kappa_g \left.\frac{\partial T}{\partial Y}\right|_{Y=0} = \rho_f \dot{r} h_v \quad (2.3)$$

Where κ_g is the gas phase conductivity, $\partial T/\partial Y|_{Y=0}$ the local boundary layer temperature gradient starting at the fuel surface, ρ_f the solid fuel density, $\dot{r}$ the regression rate of the fuel, and h_v the heat of vaporization of the fuel.

To solve for the regression rate $\dot{r}$, the aerothermal properties of the boundary layer must be approximated. A flat plate model for the boundary layer can be used and the heat transfer coefficient at the wall can be shown to be related to the skin friction coefficient via the Reynolds's analogy.

$$C_h = \frac{C_f}{2} Pr^{-2/3} \quad (2.4)$$

where C_f is the skin friction coefficient, C_h the Stanton number, and Pr the Prandtl number.

The skin friction coefficient is defined with blowing which can be described as the vaporized fuel coming off the surface of the fuel shown in Fig. II-2 as $(\rho v)_s$. The Stanton number can also be expressed in terms of heat flux, as shown in equation 2.5.

$$C_h = \frac{\dot{Q}_s}{\Delta h \rho_e u_e} \tag{2.5}$$

where $\dot{Q}_s$ was defined above as the left hand side of the equation in 2.3, Δh the enthalpy difference between the combustion flame and the fuel suface, ρ_e the density of the oxidizer at the surface of the boundary layer, and u_e the velocity of the oxidizer at the boundary layer surface. If $\dot{r}$ from 2.3 is to be solved, equations 2.4 and 2.5 can be combined and arranged as the following:

$$\dot{r} = \frac{C_f}{2} \frac{\Delta h}{h_v} \frac{\rho_e u_e}{\rho_f} Pr^{-2/3} \tag{2.6}$$

Since the skin friction coefficient C_f includes the blowing effect, the blowing effect must be quantified. C_{f_0} can be defined as the skin friction coefficient without blowing and related to the Reynolds number from boundary layer theory. The relationship can be shown as follows:

$$\frac{C_{f_0}}{2} = .0296 Re_x^{-0.2} \qquad (5 \text{ x } 10^5 \leq \text{Re}_x \leq 1 \text{ x } 10^7) \tag{2.7}$$

L. Lee in the 1950s [12] showed that the effects of blowing on skin friction could be quantified with the following equation:

$$\frac{C_f}{C_{f_0}} = 1.27 \beta^{-0.77} \qquad (5 \leq \beta \leq 100) \tag{2.8}$$

where β is defined as the blowing coefficient by equation 2.9.

$$\beta = \frac{(\rho v)_s}{\rho_e u_e \, C_f/2} \tag{2.9}$$

To finally reduce the equation for regression rate, the Prandtl number can be assumed to be nearly 1 for a turbulent boundary layer, as expected in a hybrid motor burn. The blowing coefficient can seen to be equal to $\Delta h/h_v$ when the Prandtl number is 1 via boundary layer theory. $\rho_e u_e$ is renamed as G, or the oxidizer mass flux. The final equation becomes:

$$\dot{r} = 0.036 \frac{G^{0.8}}{\rho_f} \left(\frac{\mu}{x}\right)^{0.2} \beta^{0.23} \tag{2.10}$$

where μ is the combustion gas viscosity and x is the axial position in the combustion port.

The coefficients shown are valid for calculations in English Standard Units.

In some engineering applications, a simple form of calculating $\dot{r}$ can be used that relies upon fitting the regression rate equation to experimental data rather than an analytically derived equatoin like 2.10. This equation simplified equation is as follows:

$$\dot{r} = aG_o^n \tag{2.11}$$

where a and n are free constants that can be made to fit from experimental data, and G_o is the oxidizer mass velocity that can be evaluated at any time by the oxidizer flow rate divided by the combustion port area. Any design changes in scale or additives require a suite of experiments to determine these coefficients.

This brief summary of the regression theory for classical type fuels is far from complete. It is sufficient for a somewhat close approximation of the regression rate but does not take into account all the research and modifications that have been made in this

field. For non-classical fuel or fuels with special additives, the equations can change and terms such as radiation cannot be neglected. For the purpose of this thesis, the simplest form of heat-transfer diffusion-limited regression theory is sufficient.

B. PARAFFIN REGRESSION THEORY

The bulk of the research into regression theory for paraffin-based fuels has been completed at Stanford University and Space Propulsion Group by A. Karabeyoglu with colleagues [8]. In the theory that is presented in this section is a brief summary of those efforts.

The roots of the research on paraffin fuels were from cryogenic solid fuel research in the early 1990s. Cryogenic fuels such as solid methane or solid pentane yielded high regression rates that were orders of magnitude higher than those of classical fuels. While these fuels offered high performance, they were very impractical for use in launch vehicles due to the requirements for cryogenic temperatures of the entire combustion chamber. The cryogenic research at the time never fully presented any models or theory as to how the physics behind the regression rate were able to achieve such high rates. It was not until later that Karabeyoglu and his team at Stanford began work to establish some regression theory for these fuels. It was determined that the very low heat of vaporization required for these fuels could not explain the dramatic increase in regression rate. It was postulated that entrainment of liquid droplets of fuel into the flow was a more dominant mass transfer mechanism and the reason regression was so high. This work was taken forward and paraffin based-fuels were derived that also had regression rates orders of magnitude higher than conventional fuels.

The regression theory for paraffin based fuels is significantly different than that for classical fuels. An image detailing the process is shown in Fig. II-3.

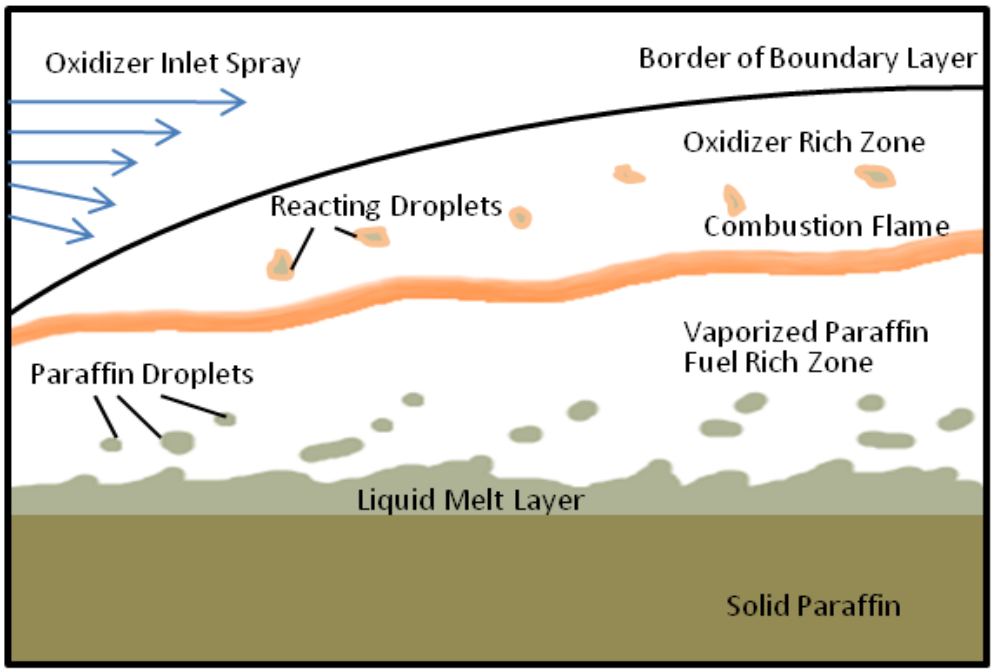

Fig. II-3 Theoretical physical model of regression for paraffin type fuels

In this process, heat is transferred through convection and radiation down to the fuel. Since the fuel has a low melting point, a liquid layer forms on the surface of the fuel. The turbulent and high velocity gas flow in the port causes the liquid layer to become unstable. The shear causes ripples on the liquid layer and due to the viscosity, small droplets are pulled up from the liquid layer and move up through the boundary layer by means of entrainment. When these droplets reach or pass the combustion flame, they themselves react in the oxidizer rich environment and burn much faster.

This new process of mass transfer requires some significant modification to classical hybrid combustion theory. The first major modification is that the effect heat of

gasification is reduced because of the entrainment effect. The second is that due to the two phase flow within the boundary layer, the blocking factor that modifies the convective heat flux is altered. Lastly, ripples formed in the liquid layer increase the surface area and roughness which enhances heat transfer.

The following regression theory and equations are summarized from the work of Karabeyoglu [8]. The regression rate for a paraffin type fuel can be broken up into two components, the regression from vaporization and the regression from entrainment.

$$\dot{r} = \dot{r}_v + \dot{r}_{ent} \tag{2.12}$$

The energy balance for a combination of entrainment and evaporative mass transfer can be written as follows:

$$\dot{r}_v + [R_{he} + R_{hv}(\dot{r}_v/\dot{r})]\dot{r}_{ent} = F_r \frac{0.03\mu_g^{0.2}}{\rho_f}\left(1 + \dot{Q}_r/\dot{Q}_c\right)B\frac{C_H}{C_{Ho}}G^{0.8}z^{-.02} \tag{2.13}$$

where

$$R_{hv} = \frac{C_l \Delta T_1}{h_e + L_v} and\ R_{he} = \frac{h_m}{h_e + L_v} \tag{2.14}$$

In these equations, C_H/C_{Ho} represents the blocking factor, μ_g the gas viscosity, ρ_f the fuel density, $\dot{Q}_r$ the heat flux from radiation, $\dot{Q}_c$ the heat flux from convection, B the blowing parameter, G the instantaneous oxidizer mass flow, z the axial distance down the port, h_m and h_e, the effective heats, l_v the latent heat of vaporization, C_l specific heat, T_1 absolute temperature, and F_r the roughness parameter.

The roughness parameter was defined by empirical formula and can be expressed as:

$$F_r = 1 + \frac{14.1\rho_g^{0.4}}{G^{0.8}(T_g/T_v)^{0.2}} \quad (2.15)$$

Where ρ_g is the gas density, T_g is the average gas phase temperature, T_v is the vaporization temperature.

The entrainment based recession rate can be expressed as:

$$\dot{r}_{ent} = a_{ent} \frac{G^{2\hat{\alpha}}}{\dot{r}^{\hat{\beta}}} \quad (2.16)$$

Where a_{ent} is the entrainment parameter, $\hat{\alpha}$ is the dynamic pressure exponent and $\hat{\beta}$ is the dynamic thickness exponent.

Equations 2.12, 2.13, 2.14, 2.15, and 2.16 form a non linear set of algebraic equations which can be used to solve the total regression rate of a paraffin type propellant as a function of axial location and local mass flux.

While these equations represent the physical explanation of paraffin regression, equation 2.11 can be used to fit a curve to experimental data and predict regression rates.

C. NON-HOMOGENEOUS REGRESSION THEORY

Regression theory for the non-homogeneous fuels of this paper take a slightly different route than the derivations for past fuels. A simplified hybrid model of regression that combines elements from both tradition regression theory such as that for HTPB and mixes in elements from modern entrainment dependent regression theory is used to try to estimate the performance of the new fuel. Results of experiments conducted in this paper will be discussed later to try to support the regression theory presented.

Before discussing the theory and proposed physical methods of mass transfer, it is important to visual what a non-homogeneous fuel looks like and what it entails. The non-homogeneous term involves multiple types of fuel mixed in a non-uniform method. For this experiment, two fuels were used, HTPB and paraffin wax. The HTPB is mixed with tiny paraffin spheres uniformly and cast into fuel cores. The two fuels are not thought to be molecularly bonded in any significant way to one another except for small thin areas around the surface of the spheres. These bonds may or may not be present, but are primarily neglected in this study. The fuel can be visualized in Fig. II-4 below.

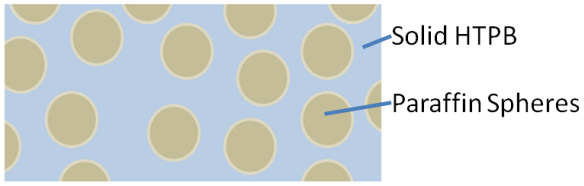

Fig. II-4 Representative cross section of the considered non-homogeneous fuel

In the non-homogeneous fuel presented in the paper, two distinct dominant methods of mass transfer of fuel into the combustion zone are theorized. The first method is vaporization of the solid HTPB fuel at the surface of the fuel through pyrolization. The second is through entrainment of small droplets of wax into and beyond the combustion region through viscous forces within the boundary layer. At first this might seem very similar to the regression theory of paraffin wax, but it differs in the fact that a liquid melt layer is not thought to be present or is very minimal due to the limited quantity of paraffin in the fuel. What is thought is that the small spheres of wax are melted at the surface of the fuel and lifted from the HTPB out into the flow where they are burned in an identical fashion as in a paraffin motor. The HTPB however still remains as a solid

fuel that regresses in the classical sense. There may however be an added benefit that results from a surface area and roughness is increase in the HTPB as the paraffin spheres are melted and pulled from the surface. Small and numerous divots will be left on the surface of the HTPB which increases the surface area and may also increase heat transfer by inducing further turbulence into the boundary flow. These benefits will be discussed later as to if they were seen or not during actual tests. A functional diagram of the basic regression is presented below in Fig. II-5.

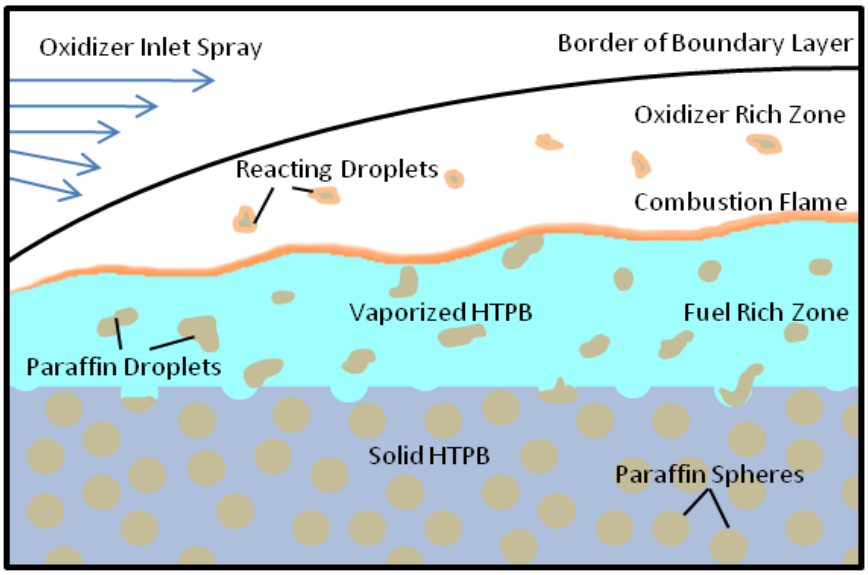

Fig. II-5 Theoretical physical model of regression for the non-homogeneous fuel

To try to quantify this regression behavior and develop a regression model, the approach of mixing the classic regression model with the entrainment based model for paraffin seemed most reasonable. Depending on the quantity of paraffin present, the relative significance of the two models could be determined and factored in. The other approach would be to use experimental data and equation 2.11 where a and n would be fit

to the data taken. This however would not be sufficient for predicting regression rates when the concentrations of the fuel were altered.

Overall, it could be said that the regression rate can be bound by equations 2.10 on the low end and by 2.12 found by the solution of the non linear series 2.12, 2.13, 2.14, 2.15, 2.16 on the high end. A rough order approximation would be to weight the each separate regression prediction by the % volume contribution near the surface of the fuel grain assuming an even distribution of paraffin spheres in the HTPB.

$$A\dot{r}_{HTPB} + B\dot{r}_{Paraffin} = \dot{r}_{total} \tag{2.17}$$

Where $\dot{r}_{HTPB}$ is equation 2.10, $\dot{r}_{Paraffin}$ is the solution of 2.12 for $\dot{r}$ and A and B are the relative percentages by volume of HTPB and paraffin wax.

Because there are two types of fuels present, the regression equations for both fuels will have some errors. In particular in equations 2.10 and 2.13, the gas viscosity μ and μ_g will not be correct since the actual gas viscosity will be a combination of gases from both fuels. The C_f in equation 2.9 needs to be adjusted for the rough surface of the HTPB which will modify the blowing coefficient. Several other equations will also be affected such as 2.15 due to a difference in gas density and 2.13 due to a modification of the blocking factor.

A higher detailed analytical model would need to be derived but was not in the scope of this experiment. What will be investigated in this paper is to determine the free coefficients from 2.11 for both HTPB and for paraffin in the test motor apparatus separately and plug those values into equation 2.17 using the weighting factors A and B.

The results of this will be compared with the actual motor burns to see if 2.17 could be a could offer a sufficiently close regression rate prediction.

D. SMALL MOTOR THEORY AND SIZING EQUATIONS

Traditionally when designing and sizing a hybrid rocket engine, a set of performance requirements are first picked to base the design on. For this investigation, a slightly different approach was taken. Due to cost constraints and the basic hardware that was already in possession, a more restricted and iterative design approach was taken. The following theory and design equations are summarized from a variety of sources and picked together to fit this project. The equations and processes used can be summarized into the following list:

- Oxidizer mass flow regulator and performance
- Fuel grain sizing and performance
- Nozzle sizing

Certain aspects of this experiment were sized and used based on their availability and ability to be purchase. Two such drivers that should be mentioned now are the oxidizer feed system and the combustion chamber outer diameter. A GOX tank with a regulator system limited to around 1585.6 kPa (230 psi) with accompanying lines limit the overall oxidizer feed performance that is covered in Section III-D. A 2.54cm (1 in) OD combustion chamber was picked due to availability of the metal and the ability to machine parts to fit with it. This chamber limits the diameter of the fuel and therefore becomes a driver in the design space.

The oxidizer mass flow regulator and performance calculations will be discussed first before the rest of the system. For all hybrid motors in general, an oxidizer feed system that can control or predict the rate at which an oxidizer flows into the engine is required. Since regression rate is highly dependent on oxidizer flow rate as seen in the previous theory sections, having unrestricted or non quantifiable oxidizer flow is not typically acceptable. There are many ways to control or limit oxidizer flow. For small engines, one of the simplest to implement is the orifice plate operating at the choked flow condition to regulate the mass flow.

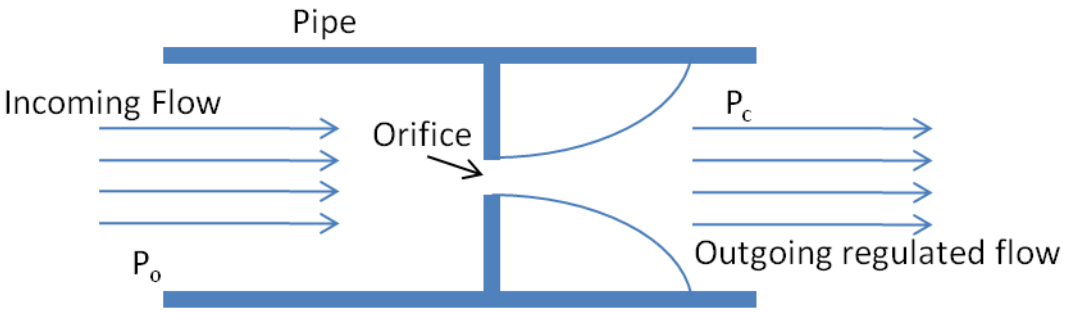

Fig. II-6 Cross section of a think plate orifice mass flow regulator

Fig. II-6 shows a typical cross section of a orifice plate style mass flow regulator. When the upstream flow is fully developed, the orifice plate can be put into the pipe to act as a restriction for the flow to pass through. A certain pressure will develop at the point P_o in the diagram due to the restriction of flow. After the orifice there will be a pressure drop at P_c associated with the increase in velocity of the flow and losses from the orifice restriction. When the downstream pressure at P_c becomes substantially low enough compared to the upstream conditions at P_o the flow can become choked. Choking occurs when the exit plane velocity reaches the sonic condition. For ideal gases this

occurs when the ratio of the upstream to downstream pressure is equal or greater to the following equation 2.18:

$$\frac{P_o}{P_c} \geq \left[\frac{k+1}{2}\right]^{\frac{k}{k-1}} \tag{2.18}$$

Where k is the specific heat ratio of the oxidizer gas being used. When this ratio is satisfied and the flow is choked, the mass flow rate of the flow can be calculated with the following equation 2.19:

$$\dot{m}_o = CA\sqrt{k\rho P_0\left(\frac{2}{k+1}\right)^{k+1/k-1}} \tag{2.19}$$

Where $\dot{m}_o$ is the mass flow rate in kg/s, C is the discharge coefficient, A is the discharge hole cross section in m^2, and ρ is the real density in kg/m^3. Most of these quantities are easily calculated on a system with the exception of the discharge coefficient. The discharge coefficient typically ranges from .6 to .8 and are difficult to approximate analytically. Design tables and other reference can be used that list orifice hole sizes with respect to the pipe size and compare the discharge coefficients as they vary with Reynolds numbers. An easier approach to determining this value is to find it experimentally by comparing the mass flow rate with an already calibrated mass flow meter if one is available.

The downstream pressure must remain low enough so that the condition in equation 2.18 is satisfied. It can however continue to decrease and the mass flow rate should hold relatively constant. What this implies in a small motor design is that the chamber pressure must remain lower than the critical value for P_c if the mass flow rate is to be

accurately known. In a less constrained situation, the input pressure P_o could be increased to a point that would allow for whatever chamber pressure is desired. In this current situation, the chamber pressure becomes limited by the supply capability of 1585.6 kPa coupled with the losses of the valving and hoses running to the orifice regulator. This effectively limits the max chamber pressure to below 620.4 kPa (90 psi) for the GOX source that is used.

Once the oxidizer flow rate capabilities have been established, the fuel grain size and length can begin to be sized. For each fuel that is used, an ideal mixing ratio of fuel to oxidizer exists. This optimum O/F (Oxidizer/Fuel) ratio is usually found experimentally but tends to exist somewhat near the point where the stoichiometric condition exists. This is the condition where the O/F ratio is such that the combustion reaction is balanced and fully complete as in there is just enough oxidizer to completely burn all the vaporized fuel. The ratio is highly idealized though since it actually varies down the length of the fuel grain due to the variance of local regression rate with length. Selection of the desired O/F ratio is highly dependent on the mission and many factors for performance that is intended to be optimized. If thrust is more highly desired, a more oxygen rich ratio may be preferable where as if the specific impulse is optimized a more fuel rich ratio may be needed. Selecting an optimized O/F ratio was not necessary nor the focus of this experiment.

The O/F ratio is found by dividing the oxidizer mass flow rate by the fuel supply rate. In a hybrid motor, this is done by determining what the regression rate of the fuel is based on the oxidizer flow rate. The regression equations presented earlier in this section

can be used to estimate this. If the regression equations are unknown or are not reliable, then this must be determined experimentally. If the regression rate is obtainable the following equation 2.20 can be used to calculate the mass production rate of the fuel in single port fuel core geometries:

$$\dot{m}_f = 2\pi\rho_f r L\dot{r} \tag{2.20}$$

Where $\dot{m}_f$ is the mass flow rate of the fuel in kg/s, ρ_f is the fuel density in kg/m^3, r is the port radius in m, L is the length of the port in m and $\dot{r}$ is the regression rate of the fuel in m/s. The total mass flow rate of the exhaust for the engine then simply becomes:

$$\dot{m} = \dot{m}_f + \dot{m}_o \tag{2.21}$$

Since this experiment was constrained to a 2.54 cm OD combustion chamber, the variable r was fixed and only the variable L could be modified to change the O/F ratio. Given that O/F wasn't to be optimized in this experiment, a value of 3.81 cm was chosen for L. This gave an O/F ratio that was typically below 2 for most tests. Forward and aft mixing chambers can also be added. There is no conclusive set of equations for sizing the mixing chambers. They are usually created based on experimentation. A way to estimate the rough size in most cases is to divide the value r by 2 and use that as the length of the pre and post mixing chambers. Uncertainty induced by this approximation was not quantifiable in this experiment.

The next critical piece to design is the nozzle. For optimum performance, a bell cone or aerospike design would be preferable but was not within the scope of the project. A traditional 15° cone is the simplest to use. For the internal cavity, a 45° cone is acceptable. For most of the sizing process of the nozzle, the isentropic relations for

supersonic nozzles can be used. The quantities that are known and can be used as the starting point for the calculations are the chamber pressure, ambient pressure and total mass flow rate. The chamber pressure is known to be less than the critical value for P_c in equation 2.18. The ambient pressure is whatever the outside air pressure is at the test site. The mass flow rate was calculated in equation 2.21. An overview of a basic isentropic flow nozzle is depicted in Fig. II-7 to aide identifying the variables associated with the equations that will follow. The P's symbolize the pressure, V's the specific volumes, A's the area and T's the temperature.

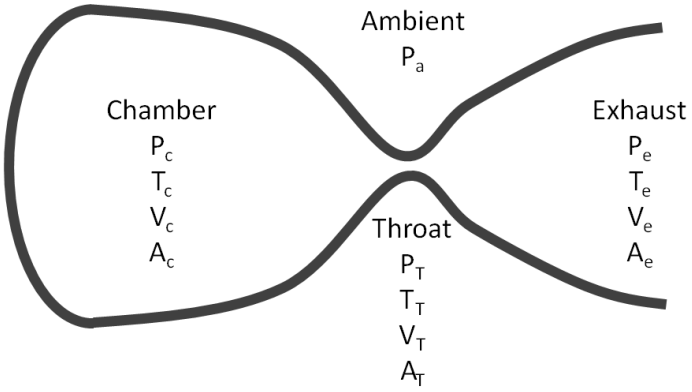

Fig. II-7 Basic supersonic isentropic nozzle

The desired quantities from Fig. II-7 to size the nozzle are the area of the throat A_T and the area of the exit A_e. Since the mixing ratio and chamber pressure are already known, it is possible to determine the specific volume V_c, and the absolute temperature T_c inside the chamber. It is also possible to determine the specific gas constant R and ratio of specific heats k. To calculate these by hand would be difficult and an understanding of the chemical equilibrium and combustion products would need to be

known. A freely available code called CEA (Chemical Equilibrium with Applications) can be used to quickly and easily find these values. Using CEA to find these values will be discussed at the end of this section. For now it is assumed that T_c, R and k have been calculated using CEA and are known. As mentioned earlier, P_c, P_a and $\dot{m}$ are also already known. The ultimate goal is to calculate A_e and A_t so that the nozzle can be sized properly.

To start, the specific volume Vc needs to be calculated. The ideal gas equation can be used and is simplified in equation 2.22.

$$V_c = \frac{RT_c}{P_c} \tag{2.22}$$

Using the isentropic relations for a supersonic nozzle, the specific volumes of both the exit and the throat can be easily calculated. Equations 2.23 and 2.24 illustrate this. Note that the value for P_e is assumed to be equal to P_a for ideal expansion.

$$V_T = V_c \left(\frac{k+1}{2}\right)^{1/(k-1)} \tag{2.23}$$

$$V_e = V_c \left(\frac{P_c}{P_e}\right)^{1/k} \tag{2.24}$$

Now that the specific volumes have been calculated, the next values that will need to be calculated are the local flow velocities at the throat and at the exit. They can be calculated using equations 2.25 and 2.26.

$$v_T = \sqrt{\frac{2k}{k+1} RT_c} \tag{2.25}$$

$$v_e = \sqrt{\frac{2k}{k-1} RT_c \left[1 - \left(\frac{P_e}{P_c}\right)^{(k-1)/k}\right]} \tag{2.26}$$

Now all the required values are needed to calculated the cross sectional area of the throat and of the exit for the nozzle. Equations 2.27 and 2.28 demonstrate how this can be done.

$$A_T = {\dot{m}V_T}/{v_T} \tag{2.27}$$

$$A_e = {\dot{m}V_e}/{v_e} \tag{2.28}$$

All of the important sizing values have now been calculated for a small hybrid motor. With these initial values, a small motor can be built with these specifications as driving parameters. While thrust was never a primary concern of this experiment, it was not used as a driving requirement in these designs. It is typically the starting point for many designs and the process for sizing a motor based on thrust requirements would lead to a slightly different approach. The thrust value however can be calculated simply with equation 2.29 and corresponding specific impulse in 2.30.

$$F = \dot{m}v_e \tag{2.29}$$

$$I_{sp} = {v_e}/{g_o} \tag{2.30}$$

The application CEA was discussed earlier to calculate some of the values such as Tc, R and k. CEA has a built-in rocket solutions application that is very useful for this. Inputs that are required are the chamber pressure, mixing ratio of the oxidizer and fuel, the molecular formula of the oxidizer and fuel, the molar enthalpy of the fuel and initial temperature of the fuel. CEA has a built in database of many fuels and oxidizers, but

certain fuels like HTPB and paraffin wax are not included. For this reason, the molecular formula and molar enthalpy must be inputted manually. For HTPB, a molecular formula of C7.337 H10.982 O0.058 and an enthalpy of 2970 kj/mol can be used. Depending the way the HTPB was cured and the quantities of catalyst and hardener these values can vary from the ones given. However the values supplied should be sufficient to get in the for initial estimation that can be iterated after testing. For paraffin, a molecular formula within the range of C25 H52 to C40 H82 with a molar enthalpy of 562 kj/mol is used. This will depend on the type of paraffin wax used. If the molecular formula is not known, an intermediate value can be used and iterated on after testing.

With the inputs setup, CEA can execute and will output the chamber throat and exit conditions. It can also output the mole fractions of the exhaust products and the performance parameter if expansion ratios are supplied in the initial set of inputs.

A spread sheet shown in Table 2-1 was developed for this experiment which combined the equations listed above with the outputs of CEA into a sizing sheet so that if changes were to be made to the motor, they could be done easily to resize the nozzle required for the individual experiment. This sizing sheet is shown below. A color code is provided to describe what values were inputted manually, which were estimated and what was calculated. The desired outputs of the nozzle sizing are shown in green.

Oxidizer Feed System (pre orifice)

Pressure (PSI)	Pressure (Pa)	Temperature (K)	Gas Constant	Density (g/L)
162	1116828	300	266	13.9

Orifice Sizing / Mass Flow Rate Calc of Oxidizer

Diameter (mm)	Discharge Coeff	Area (m^2)	k	Density (g/L)	Pressure (Pa)	mass flow rate (g/s)
1.4	0.8	1.5E-06	1.4	13.9	1116828	3.3

Fuel Regression Estimation

Weight (g)	Regression Time (s)	Fuel Mass Flow Rate (g/s)
8	4	2

CEA Inputs

Mixing Ratio	Total Mass Flow Rate (g/s)	Desired Chamber Pressure (PSI)
1.7	5.3	80

Chamber Info

Temp	Pressure (bar)	Pressure (Pa)	Gamma	M
3917	8.27	827000	1.14	13.701

Throat Info

Pressure (pa)	Temp	Area (m)	Diameter (mm)
476691	3660	1.5E-05	4.4

Nozzle

Exit Ratio	Exit Area (m)	Diameter (mm)
3.8	5.9E-05	8.6

Thrust Prediction

I_{SP}	Thrust (N)	Thrust (Lbf)
320	16.7	3.7

Measured
Determined
Calculated by Sheet
Estimated
Inputs for CEA
CEA Outputs
Desired Outputs

Table II-1 Sizing equation sheet

III. ROCKET TEST STAND

A small rocket test stand was developed to determine the regression rates and performances of the fuels discussed in previous sections. The fuels themselves are discussed in greater detail in Section IV. This section will cover the physical test stand and motor construction with corresponding requirements and iterations that were tried while developing the stand. The motor and test stand are still evolving to accommodate more features and improve operations, but the configuration used for the experiments covered in this paper will only be discussed.

A. STAND REQUIREMENTS / CAPABILITIES

Two primary sets of requirements were established and dictated the design of the test stand. The first set of requirements were for safety of the system to ensure no bodily harm during use. The second set of requirements pertained to the goals of the experiment to ensure that the required performance of the subsystems and measurement capabilities were adequate to provide meaningful results. Safety was a big priority for this experiment. Even though hybrid rockets are relatively safe, the use of a strong oxidizer and having high pressure systems can pose risk if not used properly. Therefore safety was take very seriously and a considerable effort was put into making every system as safe as possible.

The list of safety requirements used is as follows:

- Oxidizer feed system complies with safety practices listed in ASTM "Safe Use of Oxygen and Oxygen Systems" handbook.

- Oxidizer feed system utilizes several safeties to prevent backflow and has redundant shutdown solenoids.
- Electrical control board permits for automated shutdown of engine on a timer but also incorporates an emergency shutdown button.
- Engine will operate in a reasonable pressure range and have provisions to ensure sudden pressure increases will not result in an energetic explosion.
- Fuel and engine will utilize materials that are reasonably safe to handle and will not produce toxic products during or after motor runs.
- Ignition system will not be excessive to the point where igniters could cause serious bodily harm if activated by accident.
- Test stand can withstand all generated forces from a motor burn and operate safely.
- Tests must be conducted with all observers standing a safe distance and on the opposite side of the motor with respect to the exhaust nozzle.
- Standardize procedures for motor runs to ensure safe practices.

The requirements for the experiment were as follows:

- Test stand must be able to measure chamber pressure, oxidizer pre-orifice pressure and motor thrust.
- Motor cores must be able to be measured before and after burns to determine the quantity of fuel used.
- Oxidizer supply rate must be predictable and calibrated to best effort within limited budget.

- Oxidizer supply rates must be adequate to allow for a variety of oxidizer flows up to and exceeding oxygen rich for HTPB.
- Motor casing must be replaceable in case damage from heat or oxidation occurs.
- Nozzle erosion must be limited during burns and throat diameters must be known to best possible measurement with available tools.
- A data logging system is required to determine measurement vs time readings of burns.

Basic capabilities for the entire system were determined before design and construction of the test stand was started. The equations presented earlier in Section II-D were used get a rough approximation of sizing of most of the parameters of this engine. It should be noted again that optimization of performance was not a primary goal of this stand, rather regression rates over a range of oxidizer values primarily the focus. An early decision was made to use gaseous oxygen (GOX) as the primary oxidizer. This decision was made because GOX was cheaply and easily available through welding supply shops and most of the regulator hardware needed was already owned. Another early decision that was made was to use an orifice type mass flow regulation system due to cost and ease of fabrication. Oxidizer mass flow rates were desired to be within 0.9 g/s up to 3.4 g/s. The nominal chamber pressure for the engine during burns was chosen to be around 551.5 kPa (80 psi). This number was chosen for both safety and also feasibility given the cost of oxidizer supply hardware. Safety factor calculations for the chamber are discussed later in Section III-E. Since the fuels considered are not pressure dependent, 551.5 kPa seemed reasonable for HTPB but was not clear whether it was too

low for paraffin based fuels. Other small test lab motors such as those used at Stanford operate closer to 689.4 kPa. This was not quite feasible given the hardware that was available for the project. The thrust chamber pressure logging system was chosen to be capable of 3447 kPa in case there were any pressure spikes that could potentially harm the measurement instruments. Thrust logging was to be capable of at least 45 N with sufficient resolution to determine basic burn events.

B. BRIEF OVERVIEW OF INITIAL DESIGN

The initial design of the test stand and experiment can be broken down into several sub categories: oxidizer supply system, engine system and physical stand with measurement equipment. All of the final designs are talked about in more detail in the following sections. It is important to note and will be discussed in next section that most designs were completed in an iterative method based on trails.

The oxidizer supply system was designed and used to supply and regulate the flow of oxidizer into the motor during a burn. This system is critical since a predictable and quantifiable oxidizer flow is essential to get usable data out of the tests. An overview of the supply system can be seen in Fig. III-1. More detailed information about this system is discussed in section 3.4. A large pressure vessel is used to supply the system and store the oxidizer at high pressure. A pressure regulator is used to bring down the high pressure of the gas tank down to a usable range for motor burns and for safe operation with supply lines. A one-way back flow preventing valve is included in line for safety to prevent back flow into the oxidizer tank. A hand operated ball valve is also installed as an added level of safety during testing. Two solenoid valves are the final valving before

the orifice system. The solenoid valves are used to both start and stop the flow of oxidizer into the motor. When the system is shut down, the engine and oxidizer lines between the solenoid and orifice are allowed to vent to atmosphere. This feature was included to prevent excess pressure and oxidizer buildup trapped before the orifice to continue to flow into the engine after a desired shutdown.

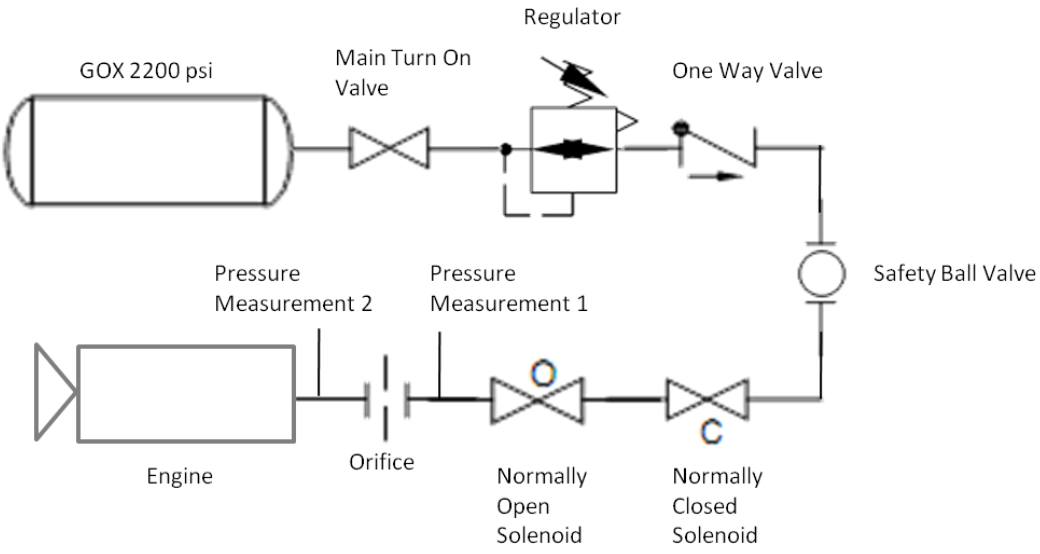

Fig. III-1 Overview of oxidizer supply system

The orifice system is a simple mass flow regulator that operates with the principles described earlier in section 2.4. A pressure tap right before the orifice is used to take measurements of the pre-orifice pressure and used in the calculation of mass flow rates. The oxidizer system details and performance is discussed in greater detail in section 3.4.

The engine system is composed of the main chamber, nozzle, fuel core and containing hardware. An initial design view of this system can be seen below in Fig. III-2. The idea was to have a system that was easily disassembled for changing nozzles

and fuel cores. It was also desired to have a pressure tap to measure the chamber pressure during a burn. Front and rear mixing chambers were also in consideration. Detailed information on this system is discussed in Section III-E.

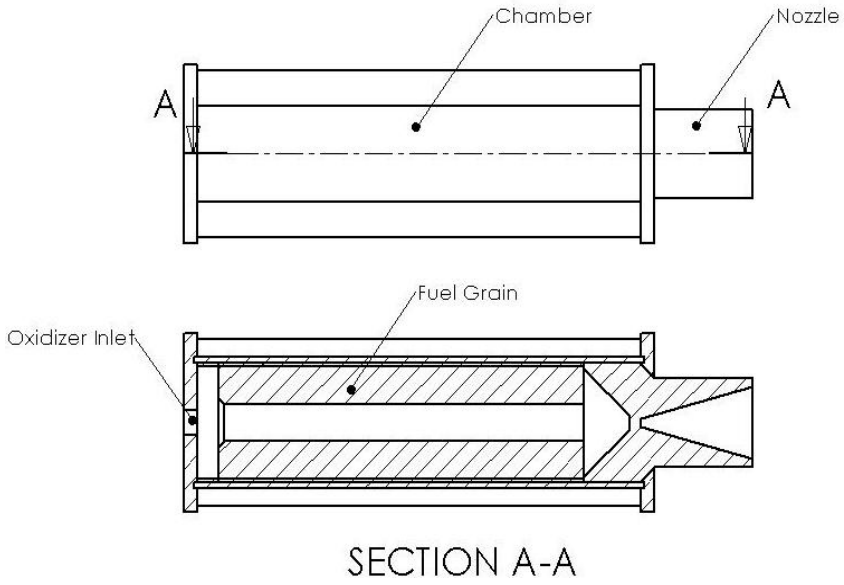

Fig. III-2 Combustion chamber overview

The test stand component of the experiment was simply a stand to hold the motor in place while allowing for thrust measurements to be taken. A sliding tray was envisioned that would allow the motor to free thrust into a load cell. The stand itself was planned to be a heavy metal plate that was affixed to a heavy concrete block to keep from moving. More information is found in section III-E on this hardware.

C. ITERATIONS

A significant amount of time was spent revising and iterating on several components in the rocket test stand. Before a more detail is given on the final configurations, it is useful to discuss some of the steps and trials that went into arriving at those designs.

A particularly time-consuming and extensive effort was put into the nozzle design for the motor. Since machining capabilities were very limited, crafting nozzles was particularly difficult. Originally the nozzles were intended to be conical and have optimized expansion ratios for optimal thrust. It was thought that nozzles could be cast in a mold and then later have a throat area drilled out to the appropriate size. This was then cut down to length for the proper exit area. A set of casting tools were made and processes for casting nozzles were investigated. These tools and cross section can be seen in Fig. III-3.

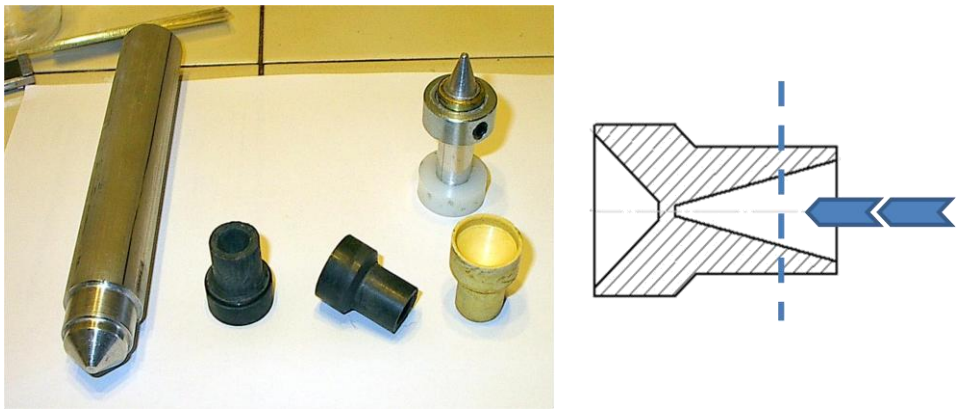

Fig. III-3 Tools for making cast nozzles and diagram of cross section for nozzle cast

These nozzles proved to be too fragile and did not seem to handle the heat in the throat area well. Cracks and failures were very common using these nozzles. During tests visible thrust direction changes could be seen as the rocket plume would abruptly change direction due to nozzle failure. A typical failure is shown in Fig. III-4.

Fig. III-4 Cast nozzle with excessive and non-symmetric erosion

Later, the nozzles were reformulated to include graphite powder, magnesium oxide and small carbon spheres. This formulation was loosely based on a hobbyist composition for solid rocket nozzles in fireworks. The mixture was much harder and more temperature resistant than the previous nozzles. They could also still be cast easily. These nozzles had a lot higher success rate than the previous but still suffered from occasional cracks and blow-outs. It was thought that small air bubbles may have existed inside the nozzles which were leading to their catastrophic failures. The biggest issue with this nozzle type, which lead to abandoning the casting method, was erosion. After successful tests using these nozzles, the area of the throat would typically erode nearly two times in size. This was unacceptable and would inhibit reliable and consistent data from burns.

A new concept for a metal machined nozzle with a graphite throat was devised. This method was favorable since thin graphite rods were very cheap and already in possession. The outer sleeve was lathed from aluminum and had several set-screws to hold the graphite center throat in place. The design was such that several tests could be performed

and if erosion within the throat became an issue, the throat could be replaced. It also allowed for the throat to be changed easily for tests where it was desired to have a larger throat, which became very common. This nozzle is shown in Fig. III-5 below.

Fig. III-5 Machined aluminum nozzle with graphite insert throat

These aluminum / graphite nozzles performed adequately for most experiments. They showed very little erosion after each test and did not exhibited the thrust alignment issues of the cast nozzles. These nozzles however developed issues later in experimenting. After repeated tests where performance was being pushed, the nozzle suffered a failure that destroyed the hardware. The O/F ratio was being pushed to levels where the engine began running oxygen rich. Naively it wasn't considered that at the elevated temperature and pressure, the aluminum would readily react with the oxygen. The aluminum portion of the nozzle was consumed by the motor and melted away as seen in Fig. III-6 with the accident and result to the nozzle. The accident did not pose risk to the operator since the failure was not explosive nor energetic.

Fig. III-6 Motor failure with aluminum / graphite nozzle and resulting damage

Due to this issue and the desire to run up into the oxygen rich O/F ratios, yet another new nozzle was devised. A 2.22cm (7/8 in) diameter graphite rod was purchased and nozzles were lathed by hand with the help of some custom made tools to achieve the correct dimensions. These new nozzles are detailed further in Section III-E.

Besides nozzle issues and iterations, there were many issues with the chamber itself that required several iterations to fix. During early tests the engine was seen (in video) to be leaking gasses from both the front and rear seals. Occasionally the chamber would also deform due to heat and reactivity with the hot oxygen. Several different types of sleeves were tried inside the motor to protect the metal chamber walls. Initially cardboard (which is common in amateur rockets) was used and was quite effective. The main issue with cardboard was that it readily burned as fuel inside the engine when the primary fuel got low. This was seen as less than ideal because the cardboard was contributing to the measured chamber pressure and thrust. The next iteration of the

sleeve was a high temperature carbon weave that was rolled into tubes and secured with epoxy. These sleeves were also very effective but only had a useful life of several tests. They were difficult to make and could become costly if they needed frequent replacement. The final solution was to use copper tube that fit snugly inside the main thrust chamber. Copper does not easily react with oxygen at high temperature and high heat. It also has a high thermal conductivity so it distributes heat away from particularly hot regions inside the engine well. Once the conversion was made to copper, failures due to lining became very rare.

The sealing issues that plagued earlier designs were remedied with higher temperature o-rings coated in high temperature thermal grease. Also, larger and thicker and plates were used with a higher thermal mass capable of absorbing more heat before rising to the critical temperature of the o-rings.

The oxidizer feed system went through significant modifications and revisions as well. Early tests had issues with the feed system lines swelling and occasionally popping apart at connections. This was alleviated by going to tougher welding supply lines. Another issue seen in early tests with the oxidizer system was when excess gas left over inside the feed lines would trickle into the engine once the engine was desired to be shut down. This extra flow would keep the engine running longer than desired and at sub optimal pressure. The result was that significant portions of fuel were slowly burnt away after the end of the test and would affect the ability to measure the regression rate reasonably. To fix this problem, different solenoid combinations were tried until eventually a setup that vented the oxidizer lines after the motor shut down was installed.

With this setup, engines shut down precisely when desired and did not continue to slowly burn afterwards. Early injector housing blocks also posed problems initially. The main oxidizer input into the injector housing was fitted in with a brass pipe fitting. During burns, the intense vibrations generated would cause the oxidizer fittings to come loose and develop slop. After repeated tightening of the fittings, the block would wear out and would not seal properly. This was fixed by making the entire injector block much thicker and adding more threading area.

The injector design itself went through much iteration. There were countless trails early on to improve the injector design. Initially it was falsely thought that the injector was causing instability inside the engine and resulting in chuffing of the motor. It was later determined that this was due to excessive leakage and wasn't noticed until it was seen on video. As a result the engine seals were fixed and the engine pressurized and checked for leaks. Optimization of the injector design at that point ceased and a simple straight forward injection area was settled upon.

The above issues and solutions mentioned above were not the only that were experienced during the evolution of the hardware. Many weekends were lost due to other issues that would arise or require solutions. Other incremental improvements were also made when money was available and access to more complicated machining techniques allowed for better parts to be made.

D. OXIDIZER SYSTEM DETAILS AND PERFORMANCE

As seen earlier back in Fig. III-1 the final oxidizer system consisted of several key components. A 15166.8 kPa (2200 psi) GOX bottle with a Matheson 3126-N/I regulator

was the feed source. The regulator was operated to its maximum open position which allowed for 1585.6 kPa of pressurized oxygen to flow. The bottle is always kept at or around room temperature of around 300 K which was typical of the inside of the garage where the tests were performed. High pressure Oxygen compatible welding lines were used as the feed lines for the rest of the system. Attached to the output of the regulator, a common backflow prevention valve was installed. After another 1.8 m, an oxygen compatible ball valve was installed as a safety option. Immediately after the ball valve, the solenoid assembly was attached. The solenoids were a MAC 113B-221JB and a Skinner V52HDA13002. The second solenoid was intended to vent the oxidizer lines between the solenoids and the motor when the motor was shut down. After the solenoids, a very short 0.3 m piece of flexible welding line attached to the back of orifice system and connected to the motor. This short piece was intended to minimize the amount of extra gas trapped behind the orifice when the solenoids were shut down. The overall assembly can be seen below in Fig. III-7.

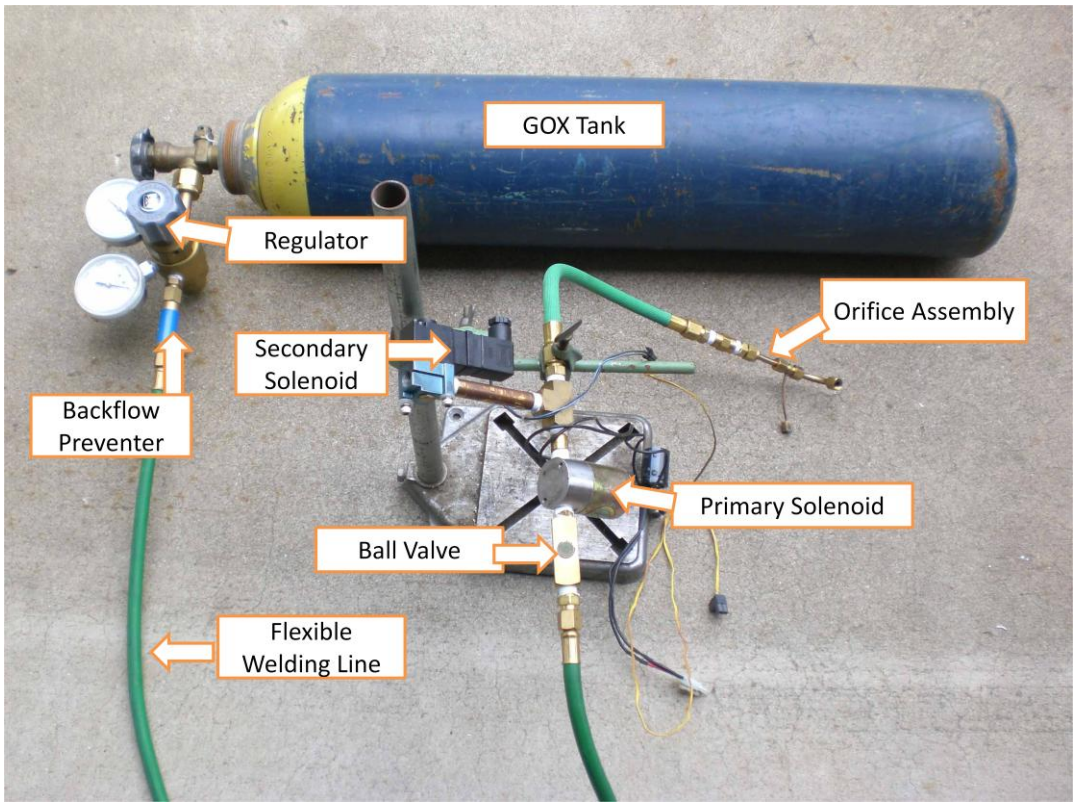

Fig. III-7 Oxidizer feed system overview

The orifice assembly was a simple choked flow style mass regulation system. It was made from brass pipe and pipe fittings. In one internal section of the assembly, small flat disks could be inserted and various size holes can be drilled into the center of the disks. Those disks act as the orifice plates. Five different disks were created with the following hole size diameters: 0.63 mm, 0.76 mm, 1.01 mm, 1.18 mm, 1.40 mm. A pressure tap was installed directly before the orifice in the assembly to allow for pressure measurements to be taken during use prior to constriction and regulation by the orifice.

A total system pressure loss analysis due to valving, hose lengths and other parasitic features was not conducted. It was not needed since the pressure of the oxidizer feed

right before the orifice was able to be measured and logged. Early test utilized an analog meter that was attached and recorded on video. Later when funding permitted, a transducer was purchased and installed to log the input pressure.

Calibration of the orifice and oxidizer feed system was done in several steps. Since there were 5 different orifices used, each orifice needed to be evaluated to determine what the corresponding mass flow rate would be. To start, the pre-orifice pressure was logged with each corresponding orifice. The logs were let run for a short period of time to reach equilibrium. The logs can be seen below in Fig. III-8.

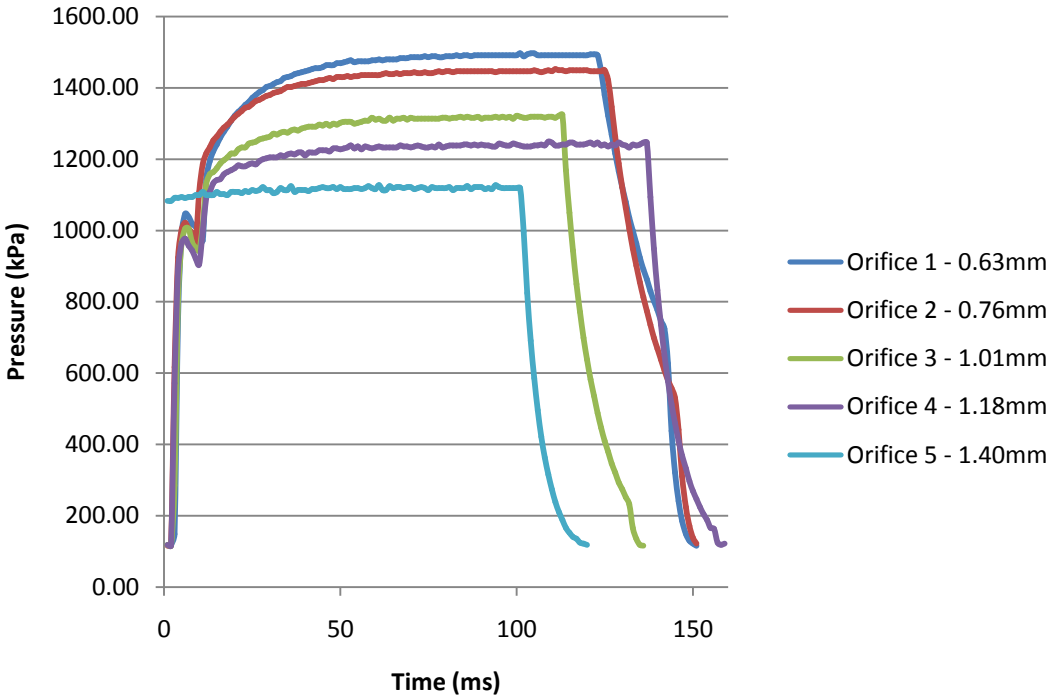

Fig. III-8 Pre-orifice pressure plots for each orifice size

With these values, the maximum chamber pressure could be calculated to ensure that the orifice would always operate in the choked condition and therefore have the mass

flow rate predicted via the equations presented in Section II-D. The results of this are presented in Table 3-1.

Max Average (kPa)				
Orifice 1	Orifice 2	Orifice 3	Orifice 4	Orifice 5
1490	1447	1317	1239	1118
Chamber Pressure Max for Chocked Flow (kPa)				
Orifice 1	Orifice 2	Orifice 3	Orifice 4	Orifice 5
787	764	695	655	590

Table III-1 Pre orifice pressure and resulting max chamber pressure

While these values are not directly important for calibration, it was critical to stay within during testing to ensure that the mass flow rates were indeed predictable. The next step in calibration was to determine the discharge coefficient of the orifice holes. This was done by attaching an in-line mounted calibrated flow meter purchased from McMaster Carr. The calibration worked by running the oxidizer system with a particular orifice installed and reading the flow rate measured by the calibrated meter. Once the flow rate was determined, the discharge coefficient could be calculated from the choked flow equation in Section II-D. The discharge coefficients were calculated to be approximately 0.8. Hence, for any nozzle at any condition the mass flow rate could be closely approximated using the choked flow equation. The results can be seen in Table 3-2.

	Orifice 1	Orifice 2	Orifice 3	Orifice 4	Orifice 5
g/s	0.9	1.3	2.0	2.6	3.3

Table III-2 Orifice mass flow rates

E. MECHANICAL DESIGN DETAILS

The mechanical design and details are split into the engine and the test stand. The engine will be discussed first.

The final configuration of the engine utilized a 2.54 cm OD chamber that could accommodate a 3.81 cm long fuel core with 0.63 cm pre and post mixing chambers. The outer combustion chamber shell was made from aluminum 2024-T3 extruded tube that was 2.54 cm OD, 0.14 cm thick and 7.01 cm long. A hoop stress analysis was calculated based on the chamber dimensions to ensure it could tolerate the operating pressures. The following equation 3.1 was used.

$$\sigma_\theta = \frac{Pr}{T} \tag{3.1}$$

Where σ_θ is the hoop stress, P is the chamber pressure, r is the internal radius and T is the wall thickness of the tube. For this alloy of aluminum, the allowable stress was around 268 MPa and the actual hoop stress of a worst case 1.37 MPa chamber pressure would be around 13.78 MPa. This means the chamber had a significant safety margin (almost 20:1).

The forward and aft mixing chambers were made from a copper tube that fit tightly into the aluminum outer tube. These 0.63 cm long tubes were in place to both hold the main fuel core in place, but also to protect the aluminum from the hot, high pressure oxygen that would react with the aluminum during combustion.

Graphite machined nozzles were created from 2.22 cm diameter graphite rod. The rod was cut into sections that were 1.49 cm long. These sections were lathed to create a 45° input cone and a 15° exhaust cone. The throat areas were tailored for each burn. A

small groove was lathed into the outer diameter at the input end to accommodate a slight overlap from the copper mixing chamber. On the exhaust end, a 0.6" diameter section was lathed down to accommodate an o-ring and permit the nozzle to be held in place by a back plate. The machined nozzles are shown below in Fig. III-9.

Fig. III-9 Graphite nozzles front and back

An exhaust back plate was machined from 0.63 cm thick aluminum plate. The incorporated a 1.6 cm diameter hole to allow the exhaust portion of the nozzle to protrude the plate. A 2.54 cm diameter 0.14 cm thick ring was cut an 0.32 cm deep into the plate to allow the combustion chamber to seat into the plate. Inside this groove a square cross section o-ring was placed to help the engine seal properly. 4 mounting holes around the perimeter of the plate permitted mounting standoffs to be used to connect the exhaust plate to the input plate and to squeeze the combustion chamber between them and permit a better seal. This plate is shown below in Fig. III-10.

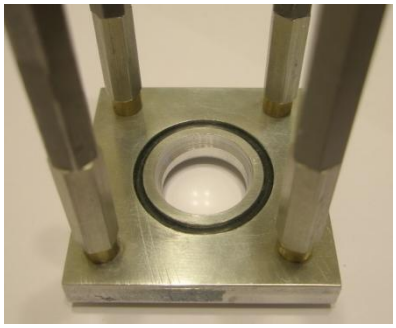

Fig. III-10 Exhaust Plate

The input side plate was constructed from 3 machined plates. This was done do to simplify and reduce the cost of machining. Two of the plates were 0.63 cm thick aluminum and the third 1.27 cm thick. The 1.27 cm thick portion was drilled to accommodate the combustion chamber within and featured a radial o-ring groove to proved extra sealing around the chamber. The central plate in the assembly has a central hole to allow oxidizer to flow through, an end sealing o-ring groove identical to the exhaust plate and a small port with fittings to allow pressure measurements to be taken inside the combustion chamber. The last plate contained all of the mounting hardware and the orifice adapter. The orifice adapter was a brass pipe thread fitting. A copper line was attached to the central plate to allow for a transducer to be mounted far enough down away as to not damage the transducer. The overall plate is illustrated below in Fig. III-11.

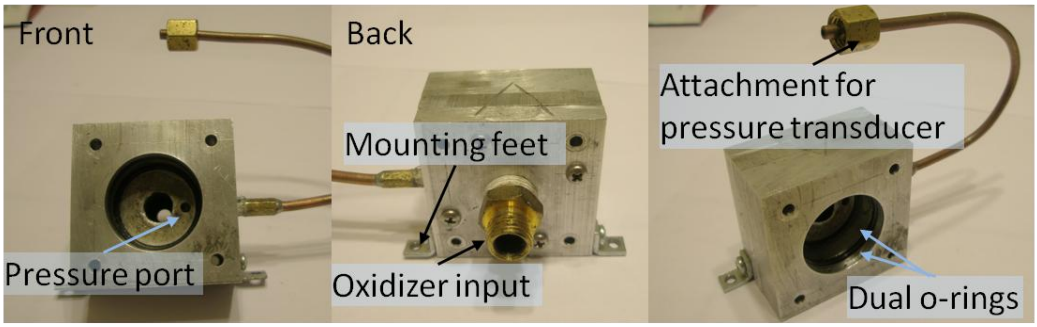

Fig. III-11 Input plate with details

The input and exhaust plates were held together by 4 chains of stainless steel standoff mounts. These mounts put a slight squeeze on the combustion chamber to force a tight seal to both the plates. The integrated pressure on the input and exhaust plates was calculated to be around 667 N considering a chamber pressure twice higher than expected for safety. Assuming 1 of the 4 standoff mounts was required to hold the entire load, it would see a axial stress of around 75 MPa. Each standoff had an axial load strength of 551 MPa (safety factor around 8:1) so they were quite capable of containing the motor during combustion. A notch was cut into 2 of the standoffs to permit a predictable way for the standoff to fail in the event of a catastrophic overpressure or detonation of the engine.

The overall engine system is shown in Fig. III-12 with all plates, fuel and chamber components displayed.

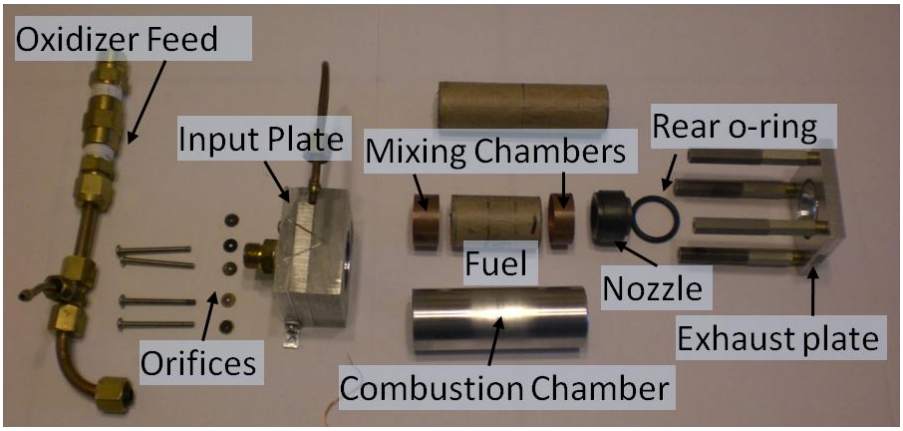

Fig. III-12 Overall engine components

The test stand itself is simply a strong mount for the motor. It has a sliding plate that the motor mounts to that allows the motor to push against the load cell during a burn for thrust measurements. The stand is constructed from aluminum and is anchored during testing to a heavy concrete block. A protective aluminum plate was also added for the unlikely situation where the engine could detonate and throw shrapnel backwards towards the operators. The sliding tray utilized Teflon blocks that was drilled out and slid on brass rods. The overall stand can be seen in Fig. III-13. Fig. III-14 shows the test stand with the motor and transducers installed.

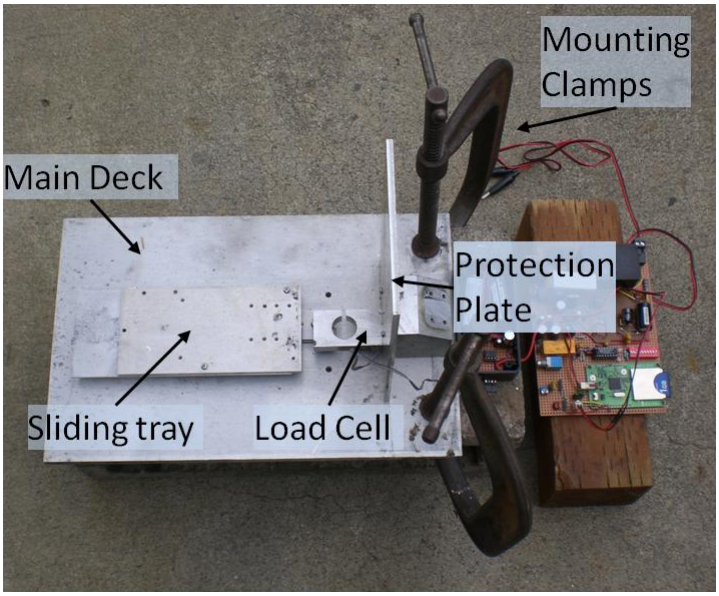

Fig. III-13 Test stand

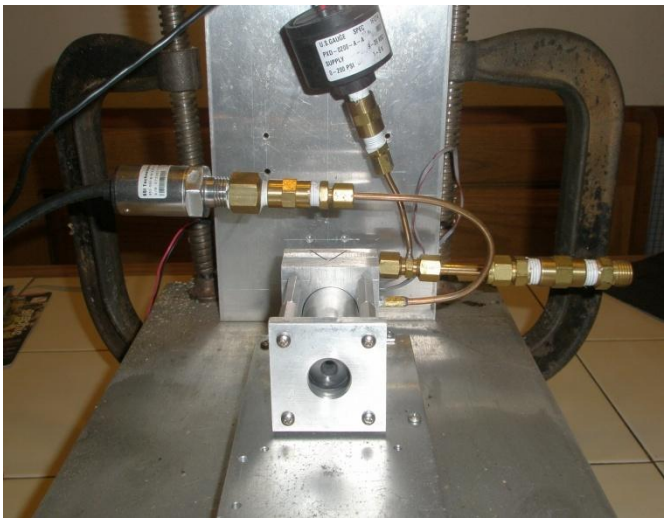

Fig. III-14 Test stand with motor installed

F. ELECTRICAL SYSTEM DETAILS

The final electrical system utilized for this experiment consisted of two primary components, motor control and data logging. Both systems were controlled by the same

control board during testing. An overview of the entire system can be seen in the block diagram of Fig. III-15. The actual hardware is shown in an overview in Fig. III-16.

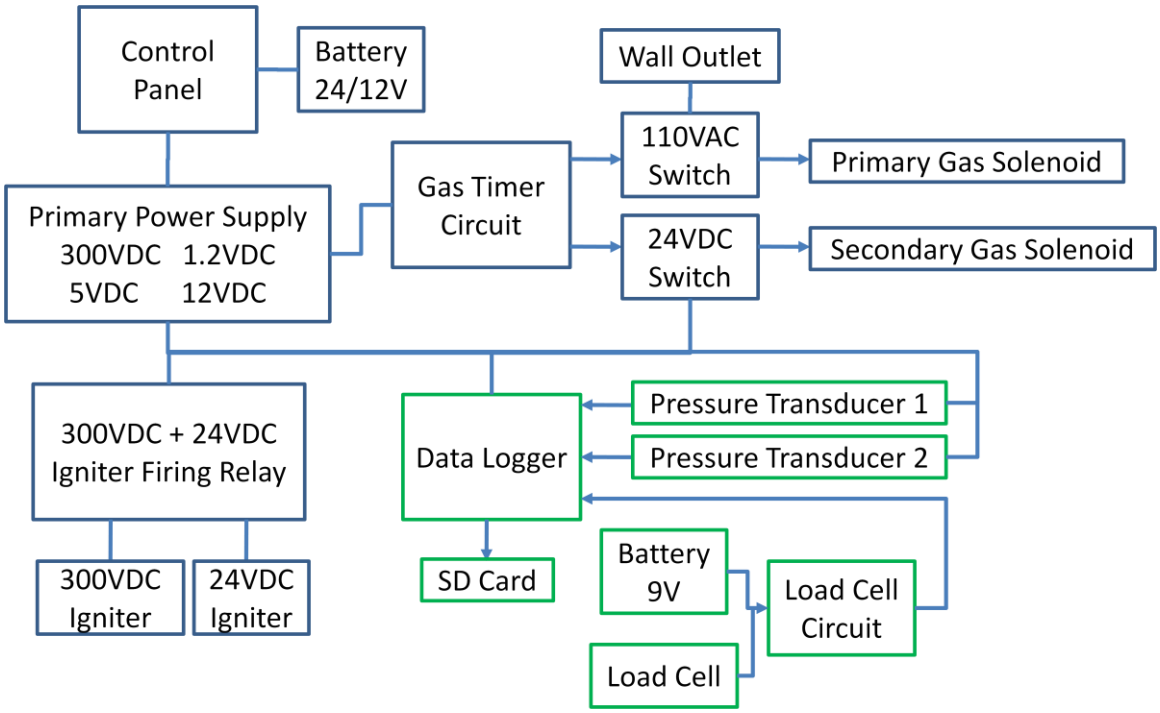

Fig. III-15 Electrical system block diagram

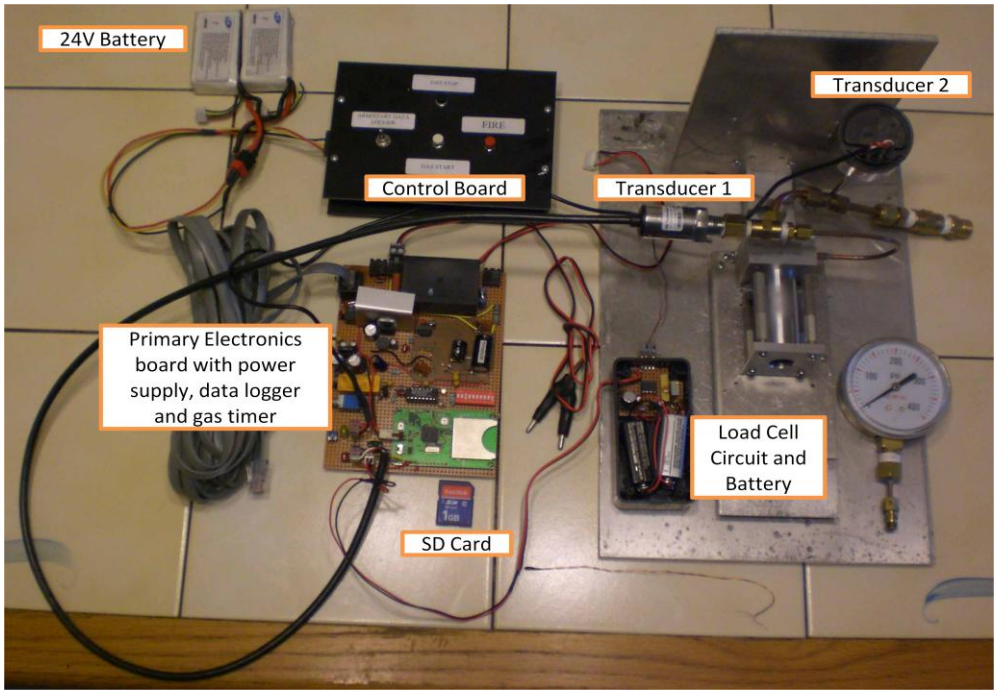

Fig. III-16 Actual electrical system hardware

A primary control board served as the operating point for the entire motor burn process. From this control board, the gas flow, data logging and ignition system could all be initialized. It is powered by the 24V battery which consists of 2 separate 3 cell lithium polymer batteries run in series. From the control board, the entire system can be energized, data loggers started, gas flow controlled and igniter fired. Typically the arming switch is flipped and a 10 second delay is used for the data logger to initialize and all systems power up. Next the gas flow would be started and after a brief moment, the igniter button fired. An internal timer automatically shuts down the gas flow after a predetermined amount of time based on predictions. In case of an emergency, or if a premature shutdown is required, the gas flow stop button can be pushed which will shut down the oxidizer flow and de-energize the system. The control panel can be seen in

closer detail in Fig. III-17 below. A 20 foot cable is used to connect the control panel to the rest of the system so the operator can be a safe distance from the motor during operations.

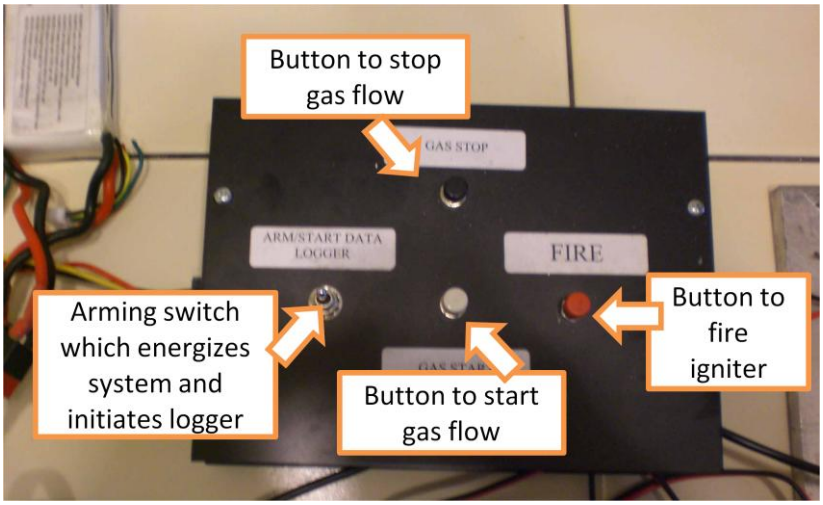

Fig. III-17 Main control board

The primary electronics board houses all the critical control circuits, power supplies and data logging components. It can be seen in closer detail below in Fig. III-18. The board sits in close proximity to the motor during operations and incorporates several LEDs that can be seen from a distance to ensure correct function during a test. All timing circuits are installed on this board and can control how long the oxidizer system is allowed to run. A simple set of DIP switches and a single POT are used to control this time.

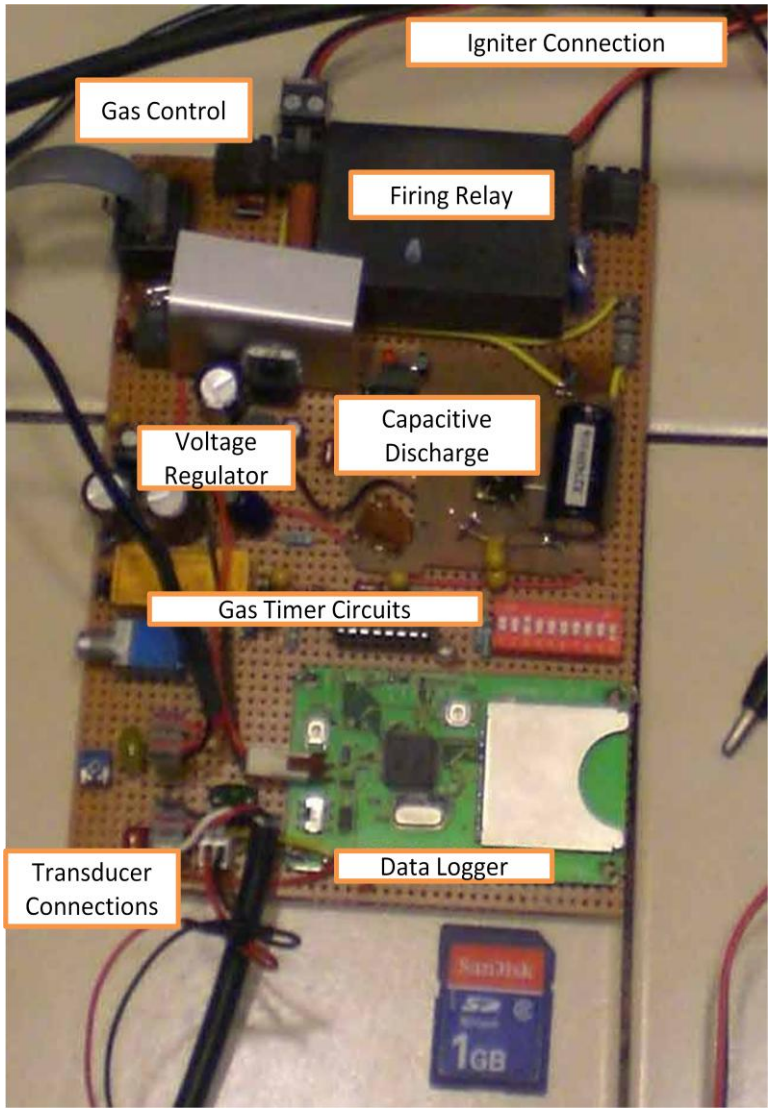

Fig. III-18 Primary electronics board

The data logger was a Sparkfun Logomatic V1 SD logger. It allowed for 10 instruments to be logged at a 0-3.3V input range. Because of this input range, the transducers needed a to have their signal lines conditioned to that range. All circuits for this were included on the primary electronics board. A 1 GB SD card was used for logging and allowed for hundreds of tests to be performed without overfilling. A scaling

system was developed for each sensor since the ADC (Analog to Digital Convervter) of the logger outputs numbers between 0 and 1024. A scale factor of volts to ADC counts was determined to be approximately 0.00322V per count. After calibration of each sensor this was correlated with a scaling factor into engineering values and stored in an Excel sheet for calculations after each burn.

The data logger collects data from two pressure transducers and the custom-built load cell. The primary transducer (which was used to log the chamber pressure of the motor during burns) was a SSI Technologies P51-500-A absolute pressure transducer. This sensor was chosen due to the scale accuracy and robust construction. The sensor was capable of ±0.5% accuracy of the full scale (3.4 MPa, 500 psi). The second transducer used to measure the oxidizer pressure (right before the orifice) was a US Gauge PXD-0200-A-A absolute pressure transducer capable of 1.37 Mpa. This sensor was chosen due to the fact that it was available to be borrowed for free for the experiment. It was just within the operating range of the oxidizer system but could potentially be damaged if the engine over pressurized and back pressurized the feed system. Both transducers were calibrated on the data logger using a custom built gas pressure test setup to within 7 Pa (~1 psi).

The load cell constructed was based on designs available freely on the internet. It consisted of a machined aluminum block with one active strain gauge and one passive strain gauge. The block was essentially a rectangular piece with a hole drilled through the large face. A slot was cut from the edge of the block and intersects the hole. A custom circuit was built to read, translate and output a signal from the strain gauges.

Based on the geometry of the block and the measurements of the strain, a load can be calculated. The circuit and load block can be seen in Fig. III-19 below. This load was calibrated with a set of precision weights ranging from 0 to 2500 grams. The result was a linear relationship and can be seen below in Fig. III-20.

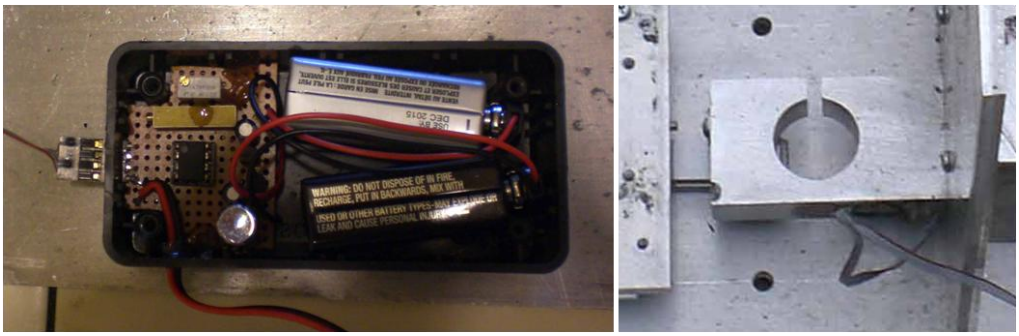

Fig. III-19 Load cell circuit and hardware

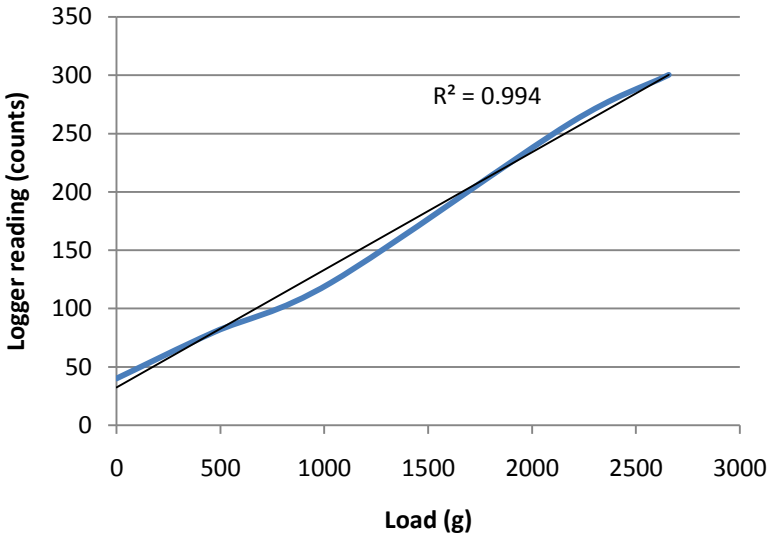

Fig. III-20 Load cell calibration plot

G. IGNITERS

The igniters were custom built to reduce the cost of each rocket test. Igniter design is roughly based on the system used to ignite Estes brand rocket engines. The igniter is composed of two major components, the burn ring and the igniter head wire. The burn ring is a small ring of Blackmatch that was cut into 2 inch lengths and tied into the ring shape. This is installed before each burn into the pre-mixing chamber of the engine. The igniter head was a bridgeless igniter with high resistance that would combust when the firing circuits were discharged through it. They were constructed of two long strands of 28 gauge enameled wire and twisting them together. The ends of the wires were tinned using a solder pot. At one end, both exposed wires were laid parallel for 6mm with 1 mm spacing between them, ensuring that no part of the wires were in contact. A thin paste of ignition material was coated on the end to join the two parallel wires. Once dried, the resistance of the wires was checked to be between 300-3000 ohms. The other end of the 28 gauge wires could then be connected to the firing circuit. The ignition wire and head was simply inserted into the motor through the nozzle throat and into the pre-mixing chamber (next to the burn ring). When current was passed through the wires at high voltage, the thin paste would explode and ignite the burn ring which in turn would ignite the engine. The composition of the ignition material was as follows:

- 16 parts potassium nitrate
- 3 parts conductive lampblack
- 3 parts -400 mesh magnesium powder
- 1 part -50 mesh aluminum/magnesium alloy powder
- 1 part -400 mesh aluminum powder

- 1 part powdered sulfur
- .1 part carbon nanospheres
- After mixing, 10% by weight nitrocellulose lacquer is added

These igniters were very effective. However, care had to be taken to ensure that they were dry before use because they would readily pull moisture from the ambient air and sometimes cause the igniter to fail. The basic igniter wire and head can be seen in Fig. III-21 below.

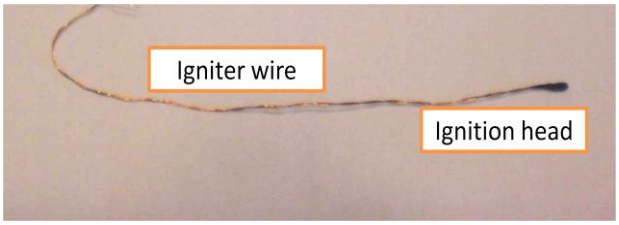

Fig. III-21 Igniter developed

IV. FUEL DEVELOPMENT

A. FUELS CONSIDERED

Four main fuel mixes were considered for this experiment. The first two represented the control cases for the experiment. A plain HTPB cast fuel and plain paraffin cast fuel were the first two fuels considered. These two fuels once tested would offer the upper and lower bounds for the experiment. HTPB would represent the lowest possible regression and paraffin the highest in the context of this investigation. Using the difference between the two as a scale, the performance of the non-homogeneous fuel could be gauged. Two different non-homogeneous fuels were developed. The first consisted of 85% HTPB and 15% paraffin by mass. The second fuel consisted of 70% HTPB and 15% paraffin. Each fuel will be discussed in more detail in the following sections. Other concepts for mixing the fuels were explored, and a few other tests were conducted with fuels such as poly(methyl methacrylate) and acrylonitrile butadiene styrene but were not included in this paper due to low relevancy to the core study.

For all of the fuels that were cast, a cardboard-like outer sleeve was made for the casting process. The sleeves were made from reinforced gummed 7.62 cm-wide packaging tape. The tape was rolled around the outside of 1.9 cm diameter aluminum tube with 7.62 cm x 7.62 cm paper note inner lining. 48.26 cm of tape was rolled around the tube tightly and let set for 1 day for the tape's adhesive to set. Each tube ended up being 7.62 cm long and fit snugly into the main combustion chamber of the rocket. Fuels were cast inside these cardboard tubes and later cut to the length of 3.81 cm.

A casting stand was constructed to properly cast the fuels with an internal core. The stand is shown in Fig. IV-1. The stand was constructed from a plastic base and drilled with a 2.22 cm hole that was 0.95 cm deep. In the center of this hole, a second 0.63 cm hole was drilled to accommodate a coring spindle. The coring spindles were 0.63 cm diameter polished brass rods. The spindles were coated with PVA mold release to enable them to be removed easily after fuel casting.

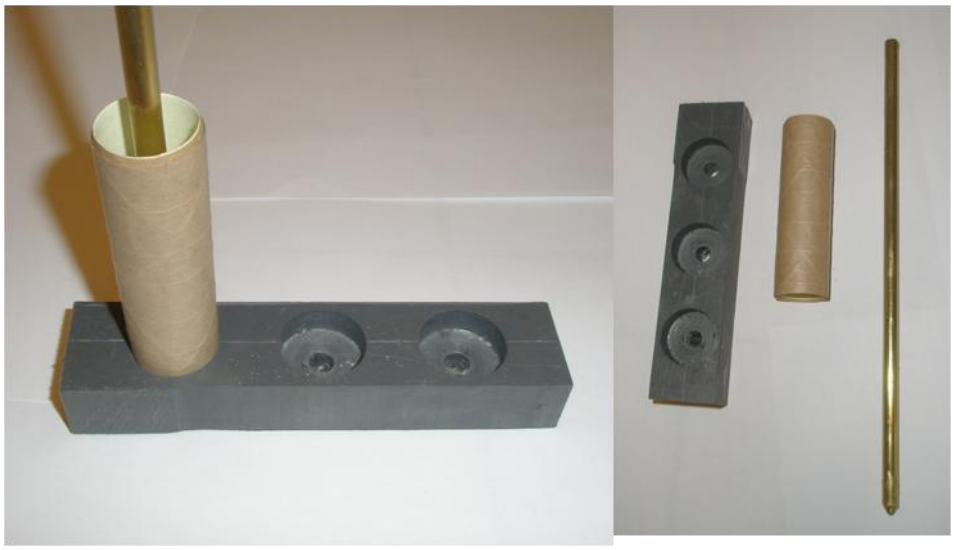

Fig. IV-1 Fuel core casting stand with fuel sleeve and coring spindle

B. HTPB FORMULATION / CASTING

The HTPB formulation and casting was the most difficult of the fuels considered to manufacture and obtain consistent results. While HTPB casting and curing is relatively common in the rocket industry, it can still be tricky to get a good cure depending on the quantities mixed in and the equipment available. Since HTPB is purchased as a very viscous liquid, it requires catalysts and curing agents to polymerize into a solid fuel. The quantities of these additives are crucial to achieve a reasonable curing time and adequate

stiffness. Several weeks were dedicated early in the investigation to determine the best mixing ratios and procedures for curing. Some of the early attempts resulted in spongy fuel or fuel with pockets of uncured liquid HTPB. Other issues involved excessive bubbles or premature curing before pouring of the motor was complete. Since the polymerization process is exothermic, monitoring the heat generation of the curing fuel was helpful to predict the correct quantity of catalyst. After many tests a suitable combination was established.

The HTPB used was the r-45m variety. The hardener that was added was Formrez SUL-4 Resin Hardener. The catalyst used was Isonate 143-L. Very fine grain carbon black was also used to make the entire fuel darker in color and to be consistent with the later fuels discussed. All of these supplies were purchased from an amateur rocket supply website. The purpose of the hardener was to lengthen the mer chains in the HTPB during curing to make the fuel stiffer, stronger and harder. The catalyst is required to start the polymerization process.

The quantities of each constituent used for each casting are as follows:

- 21 g HTPB
- 3.5cc isonate
- 0.5cc acetone
- 1/10 drop of SUL-4
- 0.06g carbon black

The process for mixing and casting was as follows:

- Pour the liquid HTPB into mixing cup.

- Add the carbon black and mix thoroughly until color is uniform.
- Add the isonate and mix very well for several minutes.
- Add the drop of SUL-4 with the acetone and allow to completely mix in a separate test tube.
- Pour the mixed SUL-4 and acetone into the HTPB mixing cup and mix for an additional 1 minute.
- Place mixing cup into small vacuum jar and de-gas for 3 minutes under 63.5 cm of vacuum.
- While fuel is degassing, prepare the casting block and cardboard tube by placing a small piece of Saran wrap over the base of the plastic block and inserting the cardboard tube into the casting hole.
- Remove the fuel from the vacuum jar and immediately pour into the cardboard tube on the casting block.
- Insert the coring spindle (pre coated in mold release) and stab it through the 0.63 cm hole in the base of the casting stand.
- Ensure the coring spindle is centered and then let fuel stand for 12 hours.
- After 12 hours the coring spindle can be removed and the fuel can be removed from the casting block.
- The fuel is put out to sit for at least 2 days to ensure complete curing.
- After 2 days, the fuel is cut to length and ready to be used.

The resulting fuel is very hard, dark and uniform in appearance. See Fig. IV-2 for the typical appearance after casting. If any anomalies or irregularities identified after

testing, the core is discarded and a new core is casted to take its place. The average density measured for the HTPB fuel cores was determined to be 965.1 kg/m^3. This is within the typical ranges seen during literature and reference searches. During inspection via dissection, it did not appear as if bubbles were a major issue inside the fuel grain.

Fig. IV-2 HTPB fuel casted

C. PARAFFIN FORMULATION / CASTING

Making the paraffin fuel cores was the easiest of the fuels to cast. The only difficulty involved in making the wax cores was the nature of the wax to shrink in volume when transitioning from liquid to solid which sometimes caused cracking inside the fuel core. This issue could be partially controlled by allowing the paraffin to cool and resolidify very slowly at room temperature. The paraffin that was selected was Parowax "Household wax" that can be purchased at most grocery stores. The specific molecular composition of the wax was not able to be determined. It was assumed it to fall within the standard range for paraffin wax of C_nH_{2n+2} where $20 \leq n \leq 40$. This paraffin wax was odorless and did not include artificial coloring. Melting point was tested before casting and was determined to be 57°C via melting plate with calibrated thermocouples. The

average measured density of this wax was determined to be 924.8 kg/m^3. Carbon black was included in this fuel mix. It had been shown by other researchers [9] that adding carbon black to the paraffin fuel can help minimize the thermal radiation through the fuel since it is normally slightly transparent. This help to prevent fuel that is further from the center core from prematurely melting and increases the local surface temperature.

The quantities of each constituent used for each casting are as follows:

- 1 block of Parowax Household Wax
- 0.06 g carbon black

The process for mixing and casting was as follows:

- Prepare the casting block by inserting a cardboard tube into the block with a small piece of Saran wrap over the base. Insert the spindle into the 0.63 cm hole in the base of the casting block and ensure it is centered up the length of the cardboard tube. Add a small masking tape ring to the top of the cardboard tube to allow for the cardboard to be over filled with fuel.
- Heat and melt the Parowax block with a heat gun letting the liquid wax collect into a mixing cup.
- Add 0.06 g of carbon black and mix thoroughly until color is uniform
- Pour the mixed wax while still liquid into the cardboard tube on the casting block and overfill into the tape ring on the top.
- Allow engine to cool at ambient room temperature for several hours.
- The fuel will have shrunk since pouring, hence the cardboard tube was overfilled and the fuel should still volumetrically fill the entire tube. If any excess was is

protruding from the top of the cardboard tube, trim excess with a razor blade and remove tape.

- Pull the spindle from the core. If spindle is difficult to remove, heat the spindle slightly with a lighter or small butane torch while pulling on the spindle. It will release and slide out easy once heated.
- Cut the fuel core down to 3.81 cm and fuel is now ready for use. Store in a cool until ready to use.

The resulting wax fuel is dark and uniform in color. When inspecting several of the sample castings, there did not appear to be any bubbles or major cracks in the fuel with the described method. Earlier test which involved rapid cooling after pouring resulted in severe cracking of the fuel core. The completed fuel core can be seen in Fig. IV-3.

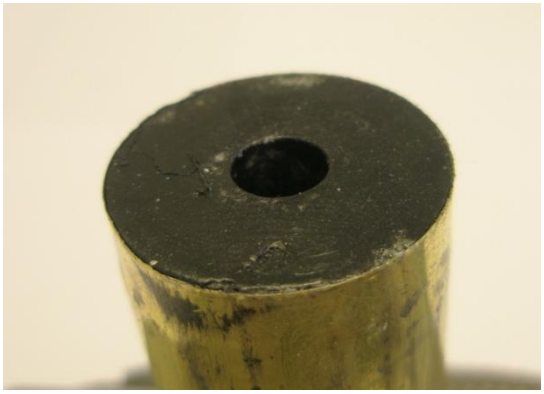

Fig. IV-3 Paraffin wax fuel casted

D. NON-HOMOGENEOUS FORUMLATION / CASTING

The non-homogeneous fuel casting utilized most of the process and mixing processes learned from the plain HTPB casting. Two different formulations were tried, one consisting of 15% paraffin by mass and the other 30% by mass. The paraffin that was

used to mix with the HTPB was unfortunately not the same as the paraffin used in the plain paraffin cores. A process for creating granulated wax of desired size and consistency was not yet implemented nor developed. In order to have uniform sized granulated wax chunks, a granulated paraffin for use in candle making was used. This paraffin wax was unscented and uncolored. As with the other paraffin used for the plain paraffin cores, the formulation was assumed to be in the typical range for paraffin wax. Melting point was tested and determined to be 61°C which is slightly higher than the previously used wax. The granulated particles were roughly 0.3-0.7mm in diameter at an average weight of $8.85x10^{-6}$g. Density of the granulated wax alone was measured to be approximately 910 kg/m^3 which is slightly lower than that of the plain paraffin used for plain paraffin wax cores. The molecular weight was close enough that results should not be heavily affected by the change of wax. Experimentation was needed to determine the best time to mix in the granulated wax to ensure a uniform mix with no bunching of particles. Carbon black was again included in the mix to keep consistent with the other fuel formulations. The process that was created is detailed below.

The quantities of each constituent used for casting the 15% paraffin fuel are as follows:

- 17.85g HTPB
- 3.15g granulated paraffin wax
- 3.5cc isonate
- 0.5cc acetone
- 1/10 drop of SUL-4

- 0.06g carbon black

The quantities of each constituent used for casting the 30% paraffin fuel are as follows:

- 14.7g HTPB
- 6.3g granulated paraffin wax
- 2.4cc isonate
- 0.35cc acetone
- 1/12 drop of SUL-4
- 0.06g carbon black

The process for mixing and casting both fuels was as follows:

- Pour the liquid HTPB into mixing cup.
- Add the carbon black and mix thoroughly until color is uniform.
- Add the isonate and mix very well for several minutes.
- Add the drop of SUL-4 with the acetone and allow to completely mix in a separate test tube.
- Pour the mixed SUL-4 and acetone into the HTPB mixing cup and mix for an additional 1 minute.
- Add the granulated paraffin wax and mix for an additional minute
- Place mixing cup into small vacuum jar and de-gas for 3 minutes under 63.5 cm of vacuum.

- While fuel is degassing, prepare the casting block and cardboard tube by placing a small piece of Saran wrap over the base of the plastic block and inserting the cardboard tube into the casting hole.
- Remove the fuel from the vacuum jar and immediately pour into the cardboard tube on the casting block.
- Insert the coring spindle (pre coated in mold release) and stab it through the 0.63 cm hole in the base of the casting stand.
- Ensure the coring spindle is centered and then let fuel stand for 12 hours.
- After 12 hours the coring spindle can be removed and the fuel can be removed from the casting block.
- The fuel is allowed to sit for at least 2 days to ensure complete curing.
- After 2 days, the fuel is cut to length and ready to be used.

The resulting fuels were dark and uniform in color, very stiff and had a uniform distribution of granulated paraffin wax. Images of the two fuels can be seen in Fig. IV-4 below. Without performing any quantifiable experiments into the structural capabilities of the fuels, it seemed (through tearing tests by hand) that the 15% mixture was nearly as resilient as plain HTPB. The 30% fuel seemed, however, to be slightly compromised in strength. The difference was not severe enough to warrant concerns over structural stability inside this small scale engine, but the fuel was noticeably easier to break apart. The strength of this mixture would need to be further evaluated for larger scale motors. Since the paraffin granules do not completely bond to the HTPB during curing, it was possible to tear portions of the fuel open and have the granules fall out of the newly

formed tear. Possible effects of this are discussed later in the results of the motor burns. Fuel density for the 15% paraffin mix was measured to be 917.9 kg/m^3 and for the 30% paraffin mix, 922.1 kg/m^3. While the average densities are roughly in the range that was expected, it is peculiar that the 30% mix had a higher average density than the 15%. This is likely attributed to the general wide variance of measured densities that can be seen later in Section VI.

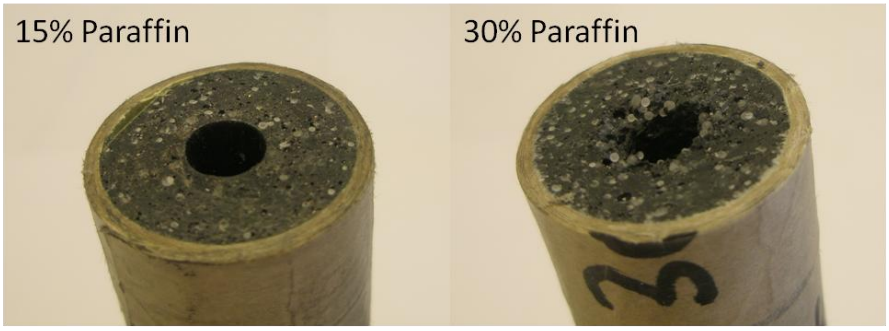

Fig. IV-4 Non-homogeneous fuels casted

E. OTHER CONCEPTS

Several other concepts were considered but due to time constraints were not fully tested or only partially investigated. One of these other concepts (in collaboration with Murbach) was a dual core design that kept the paraffin and HTPB completely unmixed. The central core would be comprised of paraffin and the outer core comprised of HTPB. The idea behind this design would have been that the central core would regress fast and give plenty of thrust. Once the inner core diameter burned out to the HTPB, the surface area inside the engine would be increased and the slower HTPB would take over and provide a longer sustaining burn. The core geometry would essentially appear as Fig. IV-5 shows below.

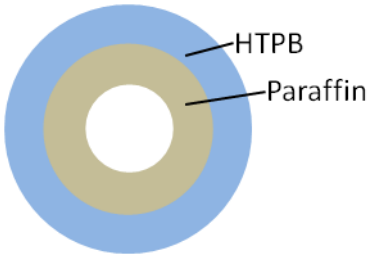

Fig. IV-5 Dual core fuel concept (Murbach & Boronowsky)

This layout would not satisfy all of the goals of the fuel development, but could potentially be a good solution for certain applications like the sounding rocket sustainer stage. Several of these fuel grains were produced early on during experimentation. Casting the HTPB in this situation was difficult without the paraffin inner core already in place. A less than ideal but suitable solution was to wrap a paraffin sheet around the coring rod for normal HTPB motor castings. This wrapped rod was then placed inside the casting blocks and HTPB was poured around it to be cured. The paraffin used was not of the same formulation as used in other tests. It's properties were largely unknown. Because of this, the tests using this fuel grain were only preliminary and only a very small number of grains were produced.

One other concept that was investigated and discussed briefly was to make a homogeneous mix of paraffin and HTPB. The homogeneous mix was created by heating paraffin to its melting point and mixing it into HTPB during the curing process while it was still thin enough to pour. The liquid paraffin acted as a thinner to the still liquid HTPB and mixed in very homogeneously. The result of the cured fuel was a very uniform and very stiff yet strong fuel grain. In order to try to determine what exactly was created in this mixing, the fuel was heated to see if paraffin would melt and escape. After

many of these tests, no paraffin could be seen escaping from the cast grain. It was thought perhaps that the paraffin formed a molecular bond with the mer chains of the HTPB during the curing process.

This new fuel would not see the benefit of entrainment that the other non-homogeneous fuels would see. This would perhaps result in slower regression rates. A small sampling of these fuel cores were produced and tested. The results confirmed that regression rate was not improved and thus this fuel was not further pursued.

V. TEST SETUP

The following sections describe the methodology and extent of the tests along with the methods used to adjust the motor for accommodating the wide variety of performances and fuels.

A. METHODOLOGY

In order for each test burn to be conducted, several parameters must be sized and a general process was followed to try to maintain consistency throughout the set of tests. The primary parameter that needed to be adjusted was chamber pressure. Due to the requirement for choked conditions of the orifice and being able to confidently estimate the mass flow rate of the oxidizer, the chamber pressure needed to be estimated and adjusted for each burn to ensure it would be below the critical value for choked flow to be predictable. This directly translated into the sizing of the throat area of the exhaust nozzle. The general methodology is outlined in the chart of Fig. V-1 below. Using this method, a series of calculations was performed to size the throat and then a motor test was performed. If the chamber pressure was acceptable and the motor functioned properly, then the test data was saved and the test repeated. The orifice could be changed for a new oxidizer flow rate and the process repeated. This process was followed for all tests that were conducted. An extensive number of practice tests were also performed to initially get the motor operating properly.

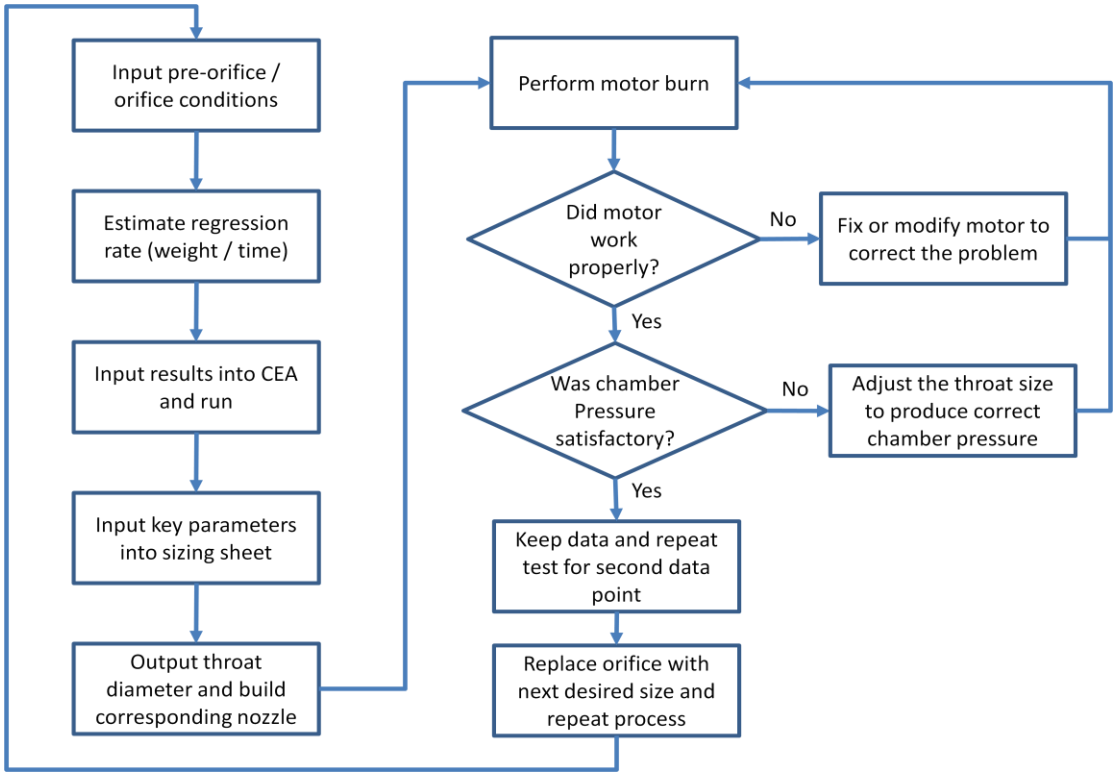

Fig. V-1 Test flow

To further clarify the steps used to control the chamber pressure, changing the size of the throat directly controls the value of the chamber pressure. In order to estimate the throat size required, the sizing sheet developed and discussed in the end of Section II-D was used. Since the sizing sheet required an estimation of the regression weight and time of the fuel to be burned and the results idealized CEA results, the sizing could not be considered truly accurate and mainly served for guidance. This resulted in an iterative method for testing the fuel. After a test, if the chamber pressure was found to be either too low or too high, the test would need to be repeated with an adjusted throat area for the nozzle. After many such tests and iterations, it became easier to estimate the throat size and not need to repeat the test.

Also included in this methodology was the provision to determine whether the motor worked properly. Each test was videotaped and monitored closely. If an anomalous sound, thrust misalignment, pressure spike or anything odd was noted during the burn, the engine would be inspected for issues and the burn repeated.

B. EXPERIMENT SUITE

There were a series of 40 tests that were to be performed and recorded for this experiment. It is important to note that, while only 40 were to be recorded for analysis, hundreds were performed to get the motor working properly and reliably. Data for those test runs were not be included in this thesis.

There were 4 types of fuel tested at 5 different oxidizer flow rates. Each test was performed two times to try to eliminate the possibility of anomalous results from motor issues or poor fuel castings. The four types of fuels tested were discussed earlier in Section IV-A. The five orifice sizes are discussed in Section III-D.

The test run matrix would evaluate the averaged regression rate of the fuel over a specific burn time. Data collected during the tests included:

- Fuel core pre-burn weight
- Fuel core post-burn weight
- Engine burn time
- Chamber pressure as function of time
- Thrust as a function of time

The main interest in these tests was the pre and post burn weight of the fuel along with the engine burn time. By subtracting the post-burn weight from the pre-burn weight,

the amount of fuel that was used during the engine could be determined. Using the time of the motor burn, the average regression rate could be calculated. Instantaneous measurement of regression rate was not possible to measure with the current suite of hardware and instruments used in this experiment.

Chamber pressure and thrust were measured mainly for verification that the engine was performing as expected. As discussed earlier, if the chamber pressure was over the critical value for choked conditions, then the data and results could not be used. If chamber pressure was too low, it was hard to confirm that the engine was sealing properly and operating correctly. The chamber pressure plots could also be used to determine if the engine is suffering from chuffing, pressure spikes or other phenomena that would indicate that motor is not operating properly. The thrust measurements were mainly measure to see if the predicted thrusts were near the measured values and if engine was behaving properly. It was not necessary for the thrust measurements to be very accurate or noise free.

C. UNCERTAINTY IN MEASUREMENTS

Due to the small scale of this test setup, many uncertainties were present that contributed to the overall error of the results. At larger scales, some of these uncertainties would play less of a role.

Most of the uncertainties in this experiment stem from these factors:

- Measurement accuracy of small dimensions (such as core diameters and throat)
- Measurement accuracy of weighed components and fuel constituents
- Machining capabilities to produce precise dimensions

At this small scale, normally acceptable measurement errors are a larger percentage of the overall quantities and play a larger role. Later in the results section, the variability in fuel density can be seen to vary around 80kg/m^3 between fuels of the same composition. Making accurate measurements of viscous fluids at this small scale is difficult and likely contributed to this measurement error. The relatively small size of the orifice holes leads to large errors in measuring the actual hole diameters. Other such issues are present in most subsystems of the experiment.

A full uncertainty analysis was not performed nor fully quantified. Due to this, the results that are presented in the following chapter must be read with the understanding that uncertainty is potentially high.

VI. RESULTS

The motor test results will be discussed in this section. Since many tests were performed including many preparatory, the data from all could not be presented due to length. The raw data and video logs of each measured test were accumulated and stored. Summary tables of the data are presented in Section VI-B.

Tests of HTPB and the two mix fuels went fairly smoothly after all the improvements to the basic motor were completed. The plain paraffin wax tests, however, were not as successful. Only 4 tests were recorded and the resulting data was not as consistent. The possible reasons for this will be discussed in further detail later in this section, but the main issue was perhaps due to the low O/F ratio and insufficient oxygen for a stable burn. The tests of the 70% HTPB 30% Paraffin had an audible coarse sound as compared to other burns, but did not reflect any issues in the plots of chamber pressure and thrust. It is possible that this sound was due to small chunks of paraffin being ejected from the motor without being completely burnt.

A. EXAMPLE TEST RESULTS

A test of plain HTPB is shown below in Figs. 6-1 through 6-3 and in the following tables. This test is representative of the bulk of tests that were conducted.

Test:	HTPB-5b	Fuel:	HTPB	Orifice:	1.4mm	
Throat:	3.4mm	Notes:	Clean flame, no issues			

Table VI-1 Burn Parameters

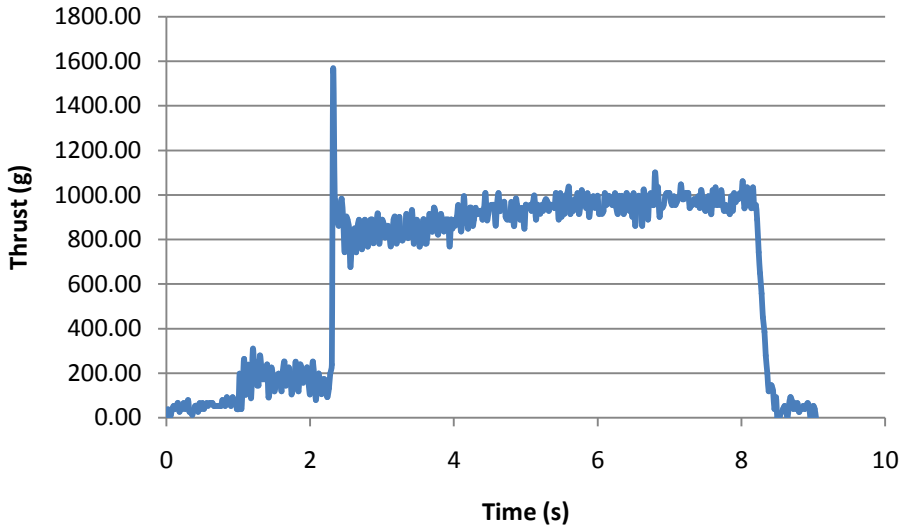

Fig. VI-1 Thrust curve

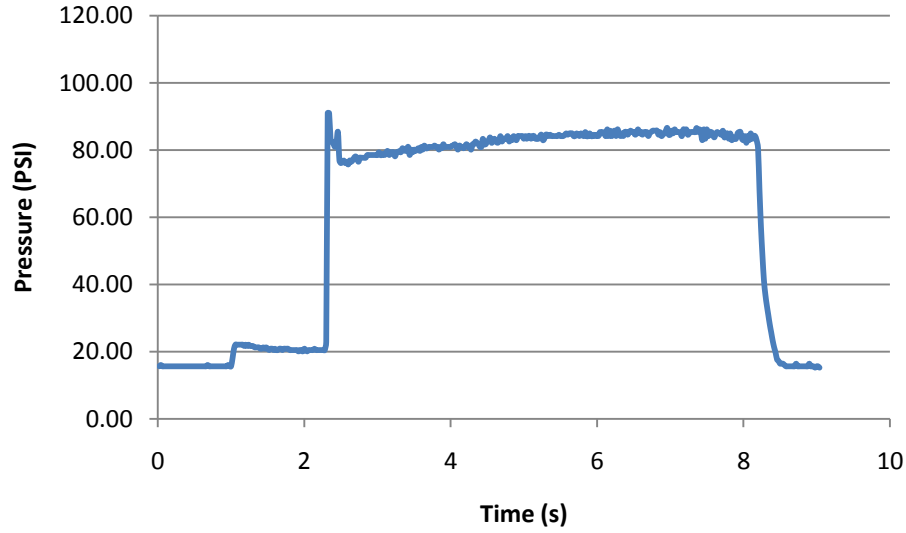

Fig. VI-2 Chamber pressure curve

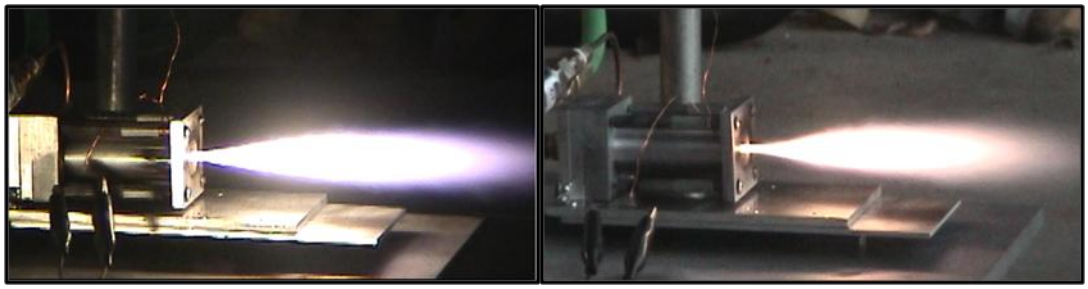

Fig. VI-3 Typical clean burns for HTPB and mixed fuels

Oxidizer Flow Rate	G_0 Start	G_0 End	Initial Fuel Weight	Fuel Quanity Burned	Burn Time	Fuel Density	Average Regression Rate	Average Regression Rate
g/s	g/mm^2-s	g/mm^2-s	g	g	s	g/mm^3	g/s	mm/s
3.3	0.10	0.013	12.35	7.66	5.88	9.92E-04	1.31	0.95

Table VI-2 Recorded data and rates from test

As mentioned in Section V-B, the beginning and end weight of each fuel core was measured and cataloged. The oxidizer rate was established from Section III-D and also logged. The G_o start and G_o at the end of the burn can be calculated using the oxidizer flow rate divided by the fuel port area at the begging and end of the run. Fuel density was calculated using by dividing the weight of the entire fuel core, minus the cardboard sleeve, by the size of the fuel core cut. Average regression rates were calculated in both g/s and in mm/s. The g/s calculation was done by dividing the fuel quantity burned by the burn time. The mm/s calculation was done by dividing the change in radius of the fuel core by the burn time. Burn time was established from the plots of chamber pressure.

If the plot of thrust is investigated, several key events and trends can be seen. Fig. VI-4 illustrates these items.

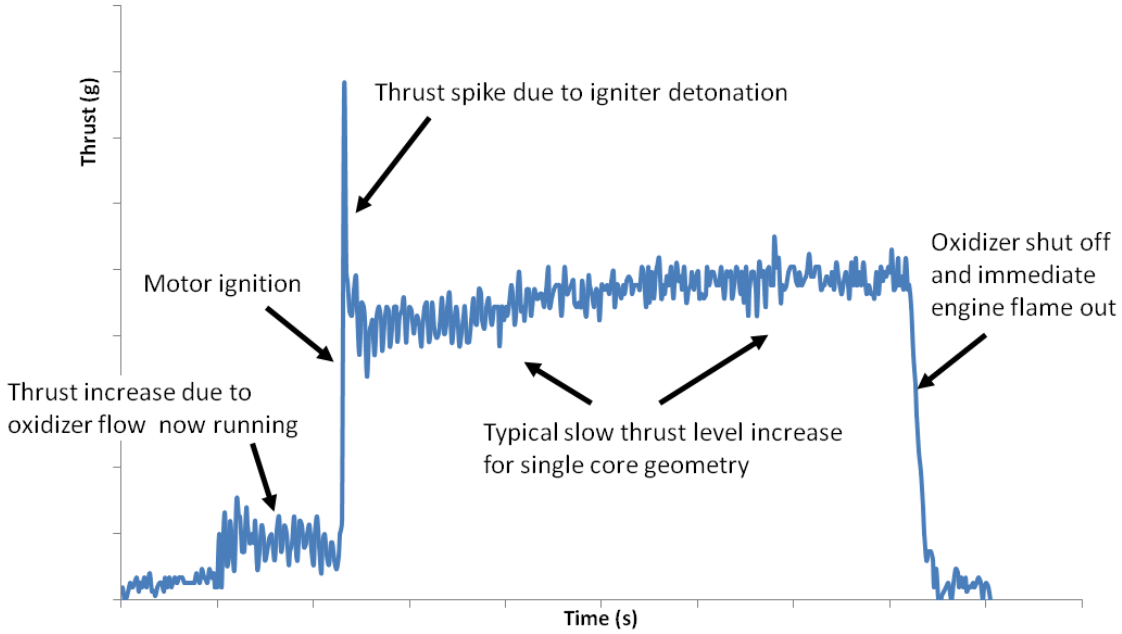

Fig. VI-4 Phenomena of the thrust plot detailed

As shown, the major events of the motor test procedure can be seen. The slight thrust level rise from the oxidizer flow being initiated is shown on the far left. The motor ignition and accompanying thrust spike is shown. The sharp cut off when the oxidizer flow is stopped is evident. The sharp spike during motor ignition is due to the igniter detonation. The igniter generates a rapid amount of heat and gas when it ignites and burns very rapidly in a GOX environment. This rapid expansion of gas and heat produces a temporary boost in thrust. The slow thrust level increase seen is typical for any type of solid or hybrid motor that utilizes a single core geometry. The reason for this is the surface area will continually increase inside the fuel grain as the burn progresses.

Due to the increase in surface area, the mass flux of fuel increases and in turn increases thrust. The thrust plot is seen to have noise in it. This is not due to motor instabilities or thrust oscillations, rather just due to the noisy nature of the circuits and sensor and vibrations from the acoustic environment during a burn.

The next image, Fig. VI-5, details the phenomena seen in the pressure plot for the motor burn.

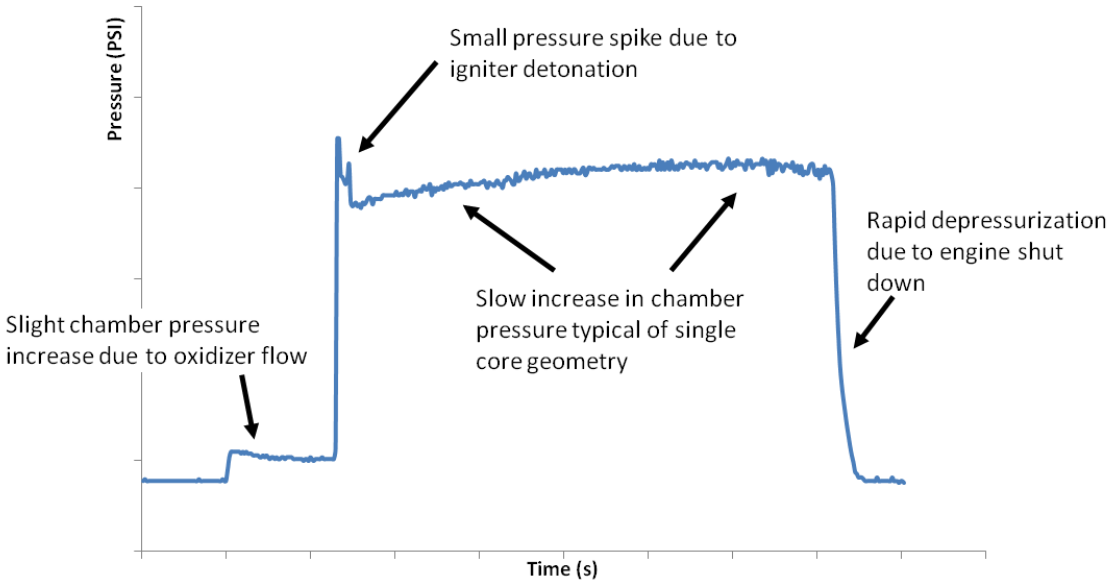

Fig. VI-5 Phenomena of the chamber pressure plot detailed

The same major events that were previously indicated for the thrust plot are seen at the same key times in the chamber pressure plot. The pressure plots are relatively smooth and seem to indicate that the burn was stable and was not chuffing.

B. TABLUATED TEST DATA

A summary of all the motor burns are included in the following tables and separated by the type of fuel that was used.

HTPB Pure

			Measured					
Oxidizer Flow Rate	G_0 Start	G_0 End	Initial Fuel Weight	Fuel Quantity Burned	Burn Time	Fuel Density	Average Regression Rate	Average Regression Rate
g/s	g/mm^2-s	g/mm^2-s	g	g	s	g/mm^3	g/s	mm/s
0.9	0.028	0.0052	11.62	4.76	6	9.18E-04	0.79	0.70
0.9	0.028	0.0059	11.82	4.24	5.76	9.38E-04	0.74	0.66
1.3	0.040	0.0069	11.76	5.24	5.84	9.32E-04	0.90	0.77
1.3	0.040	0.0082	12.24	4.51	5.86	9.80E-04	0.77	0.66
2.0	0.064	0.011	12.53	6.07	7.72	1.01E-03	1.06	0.61
2.0	0.064	0.0095	11.6	6.2	5.38	9.16E-04	1.08	0.95
2.6	0.083	0.012	12.29	6.82	5.84	9.86E-04	1.27	0.89
2.6	0.083	0.011	12.02	7.08	5.72	9.59E-04	1.21	0.95
3.3	0.11	0.015	12.6	7.33	5.72	1.08E-03	1.28	0.93
3.3	0.11	0.014	12.35	7.66	5.88	9.92E-04	1.31	0.95

Table VI-3 HTPB Pure test data

85% HTPB 15% Paraffin

			Measured					
Oxidizer Flow Rate	G_0 Start	G_0 End	Initial Fuel Weight	Fuel Quantity Burned	Burn Time	Average Fuel Density	Average Regression Rate	Average Regression Rate
g/s	g/mm^2-s	g/mm^2-s	g	g	s	g/mm^3	g/s	mm/s
0.9	0.028	0.0055	11.70	4.48	5.27	9.26E-04	0.90	0.76
0.9	0.028	0.0052	11.47	4.77	5.26	9.03E-04	0.85	0.81
1.3	0.040	0.0086	11.94	4.10	5.04	9.51E-04	0.81	0.73
1.3	0.040	0.0061	11.45	5.87	5.28	9.01E-04	1.11	0.94
2.0	0.064	0.0084	11.64	7.25	5.16	9.20E-04	1.40	1.09
2.0	0.064	0.0091	11.63	6.59	5.00	9.19E-04	1.32	1.06
2.0	0.064	0.011	11.58	5.00	3.94	9.14E-04	1.27	1.11
2.6	0.083	0.014	11.76	5.48	3.86	9.32E-04	1.42	1.20
2.6	0.083	0.014	11.64	5.25	3.92	9.20E-04	1.34	1.15
3.3	0.11	0.015	11.39	6.29	3.86	8.95E-04	1.63	1.35
3.3	0.11	0.015	11.59	6.45	3.82	9.15E-04	1.69	1.37

Table VI-4 85% HTPB 15% Paraffin test data

70%HTPB 30% Paraffin

			Measured					
Oxidizer Flow Rate	G_0 Start	G_0 End	Initial Fuel Weight	Fuel Quantity Burned	Burn Time	Average Fuel Density	Average Regression Rate	Average Regression Rate
g/s	g/mm^2-s	g/mm^2-s	g	g	s	g/mm^3	g/s	mm/s
0.9	0.028	0.0060	11.67	4.07	3.86	9.23E-04	1.05	0.97
0.9	0.028	0.0063	11.85	3.90	3.90	9.42E-04	1.00	0.92
1.3	0.040	0.0075	11.66	4.70	3.90	9.22E-04	1.21	1.07
1.3	0.040	0.0076	11.69	4.61	3.90	9.25E-04	1.18	1.05
2.0	0.064	0.0094	11.57	6.27	3.92	9.13E-04	1.60	1.31
2.0	0.064	0.010	11.55	5.76	3.80	9.11E-04	1.52	1.28
2.6	0.083	0.012	11.77	6.24	3.92	9.33E-04	1.59	1.29
2.6	0.083	0.013	11.84	6.06	3.86	9.41E-04	1.57	1.27
3.3	0.11	0.012	11.58	8.08	3.80	9.14E-04	2.13	1.61
3.3	0.11	0.0120	11.41	8.18	4.02	8.97E-04	2.04	1.55

Table VI-5 70% HTPB 30% Paraffin test data

100% Paraffin

			Measured					
Oxidizer Flow Rate	G_0 Start	G_0 End	Initial Fuel Weight	Fuel Quantity Burned	Burn Time	Average Fuel Density	Average Regression Rate	Average Regression Rate
g/s	g/mm^2-s	g/mm^2-s	g	g	s	g/mm^3	g/s	mm/s
1.3	0.040	0.0093	11.72	3.59	1.12	9.28E-04	3.21	3.04
2.0	0.065	0.011	11.70	5.20	1.38	9.26E-04	3.77	3.24
2.6	0.083	0.010	11.62	7.68	2.18	9.18E-04	3.52	2.70
3.3	0.11	0.011	11.70	9.51	2.36	9.26E-04	4.03	2.86

Table VI-6 100% Paraffin test data

C. REGRESSION DATA PLOTS AND DETAILS

A plot of all the tests is shown in Fig. VI-6 to detail the regression rate as a function of oxidizer mass flux.

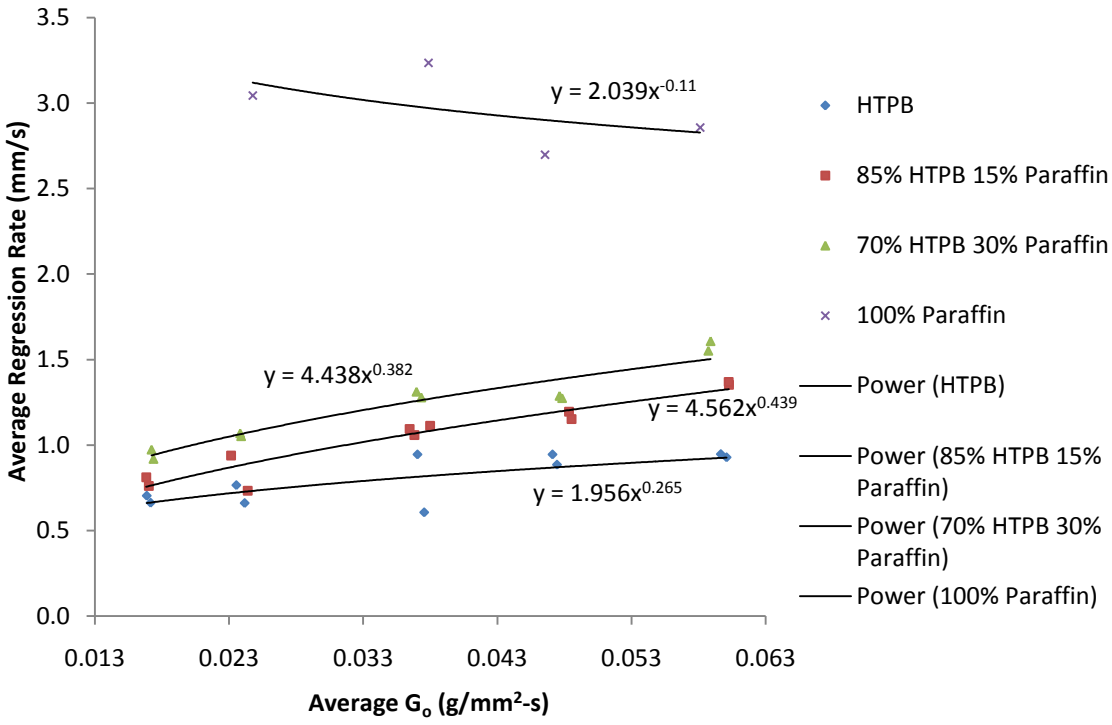

Fig. VI-6 Regression data as function of average oxidizer mass flux

This plot represents the main results of the experiment. To note, there are several irregularities in the data. Several data points in the plain HTPB and in the 70% HTPB 15% paraffin do not conform to the overall trend of the series. Also, the data for the regression rate of the paraffin shows a negative trend which is not typical. It must be noted that no time dependent measurements were taken of regression. All data is averaged over the length of the fuel burn.

The first notable result from this data is that the mix fuels did indeed perform better in terms of regression rate than plain HTPB. As expected, the higher concentration paraffin fuel regressed faster than the lower concentration mix. The regression rate of paraffin was much higher than that of the other fuels as expected.

The data as a whole has some major trends that need to be discussed. As mentioned there are several irregular datum points for the mix fuels and for HTPB. In particular the two data points at the third orifice value for HTPB are substantially different from one another. The plots of data for these runs do not show any irregularities. Chamber pressure during these runs was slightly higher than normal runs by approximately 69 kPa, but should not have contributed to the odd result. It is possible the fuel in these runs was not fully cured or there may have been debris in the orifice during the burn. In any case, they do not seem to affect the trend of the data too substantially. There are a few more data points like this in the 70% HTPB 30% paraffin, but reason for discrepancy is perhaps similar.

A more substantial and more interesting result is that the paraffin regression curve shows a negative value for the exponent in its fit power curve. This is not typical nor was

it expected. There were only a few data points for the paraffin tests due to an inability to get the motor to run properly. This could be due to several reasons but is likely why that data is not showing what would be expected. The paraffin burns in general were seen to chuff, blow out, have excessive secondary detonations or operate without any visible flame in the exhaust (with excess smoke). Some of these results are compared in the images of Fig. VI-7.

Fig. VI-7 Paraffin burns contrasting clean vs poor burns

Several factors may have been at play with the paraffin tests. The first was that the thermal mass of the paraffin fuel was relatively small. With the intense heat generation of the motor and the low melting point of the paraffin, it is possible the melt layer formed in the fuel was much too great and the conduction of heat through the fuel was large and detrimental. This may have cause an excess of fuel or liquid to disrupt the flow in the motor and cause the burn to become unstable. The next and likely more substantial reason for the issues was that the O/F ratio for the paraffin fuel was very low. It was within the range of .1 to .8 depending on the particular test. This may be too low for a burn to maintain stability. All the tests with corresponding O/F ratios can be seen below in Fig. VI-8.

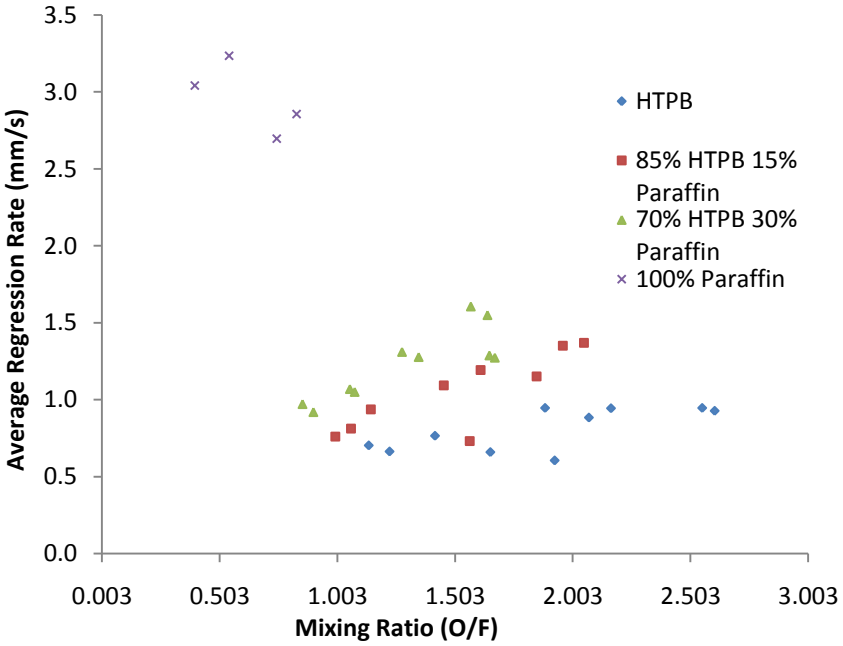

Fig. VI-8 O/F ratio for all tests plotted against regression rate

The 4 tests that were recorded for the paraffin were the most stable of the many burns that were attempted with this fuel. The first two tests at lower oxidizer rates ran for over 1 second before becoming unstable and blowing themselves out. The other two burns lasted much longer and where shut down to prevent burning into the cardboard. This suggests that the issue may indeed be related to the low O/F ratio.

The negative trend of the data may be a result of the burn time and the way the data is averaged. For all the other fuels tested, it was attempted to enable the fuel to burn to the point where no fuel would be left. Because of this, the tests utilizing lower oxidizer fuel rates ran for much longer than those at higher oxidizer fuel rates. In the paraffin tests, the two results at lower oxidizer rates ran for shorter than their higher oxidizer rate counterparts. During the initial part of the burn, the oxidizer mass flux G_o was much

higher than during the latter parts of the burn since it is calculated by dividing the oxidizer flow rate by the port area. When the G_o is higher, the overall regression rate as defined by equation 2.11 will be higher. Since port area fits an exponential curve as seen in Fig. VI-9, the G_o value will rapidly shrink in value as the port radius burns outward in an exponential manner.

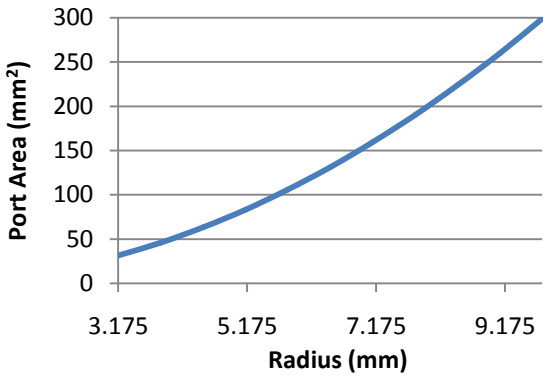

Fig. VI-9 Port area as a function of port radius

Because of this reason, and because the regression data is averaged over the entire burn and is not take in a time dependent fashion, the shorter burns will see an averaged higher regression rate than their longer burning counterparts. This is a major issue for analyzing the data with averaging methods. If the regression Fig. VI-6 is re-created but, instead of using the averaged G_o value, the end of burn G_o value is used, that data looks closer to what was expected. This is shown below in Fig. VI-10.

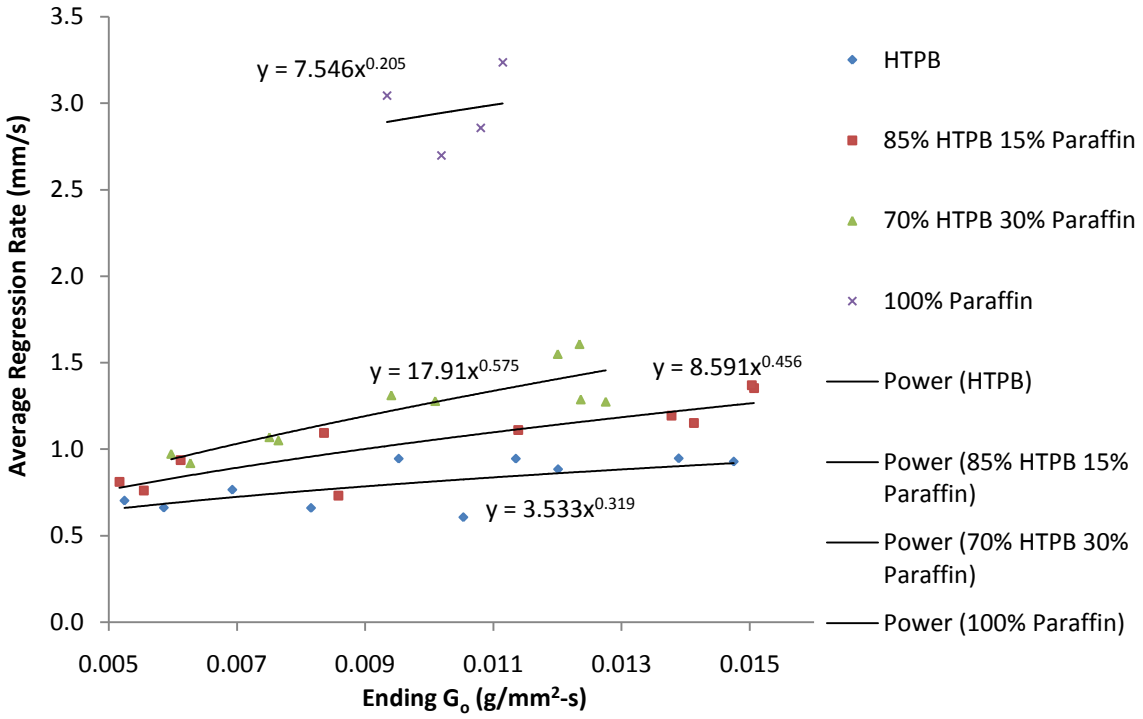

Fig. VI-10 End of burn oxidizer mass flux plotted against regression rates

Here the paraffin data is now looking closer to published trends but is still not considered accurate. Since the first two data points have an oxidizer mass flux at a much smaller port diameter, the data would not be able to be correlated properly. Because of this, it would be difficult to determine if the theorized equation 2.17 is a good approximation or not.

D. REGRESSION EQUATIONS AND PERFORMANCE SUMMARY

For the average regression data using the average oxidizer mass flux, the regression equations can be summarized in with following Table 6-7.

Fuel	Regression Equation
HTPB	$1.956G_o^{0.265}$
85% HTPB 15% Paraffin	$4.562G_o^{0.439}$
70% HTPB 30% Paraffin	$4.438G_o^{0.382}$
100% Paraffin	$2.039G_o^{-0.11}$

Table VI-7 Calculated regression formulas

As mentioned before, the paraffin data was unreliable so the regression equation has a large uncertainty. The percentage increase in regression rate over HTPB was plotted vs oxidizer mass flow to show the benefits of mixed fuel in Fig. VI-11.

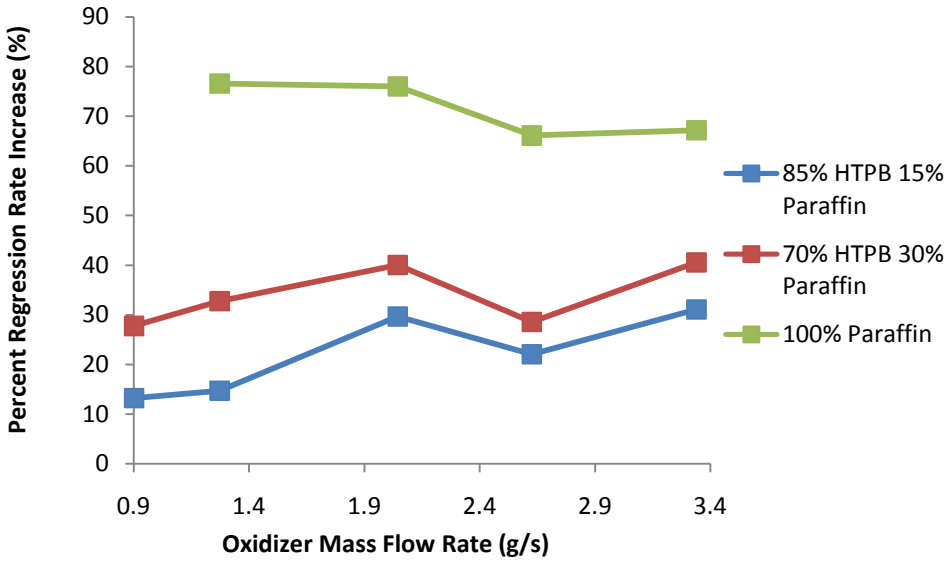

Fig. VI-11 Percentage increase in performance over standard HTPB

The mixed fuels offer a substantial increase in regression rate over standard HTPB. What is interesting is the dip around 2.6 g/s oxidizer flow. Both mixed fuels showed a reduction in performance compared to their overall trend. The reason for this is not currently known, but may be a result of the limited amount of data and some anomalous results due to factors that weren't accounted for. It is possible the orifice for that test was

slightly damaged after the first runs with HTPB and each subsequent test with that orifice was affected. After inspection of that particular orifice, it was not clear if this was the case. This discrepancy could be a result of the high uncertainty in a small motor like and could imply the overall results are questionable.

In Section II-C, equation 2.17 was proposed to be used to predict the regression rate of the mix fuel. The equation called for two coefficients based on the volumetric weighting of each regression weight. The equation reiterated below.

$$A\dot{r}_{HTPB} + B\dot{r}_{Paraffin} = \dot{r}_{total} \tag{6.1}$$

The components of regression for HTPB and for paraffin are now known. However, the components for paraffin have a higher uncertainty. The weighting factors A and B are calculated for each mix fuel type based on the volume. Since the densities of the HTPB and paraffin are close to 1, these weighting factors are close to the mass percentage. For the 85% HTPB 15% Paraffin mix, A = 0.843 and B = 0.157. For the 70% HTPB 30% Paraffin mix, A = 0.688 and B = 0.312. Equation 6.1 is split into equations 6.2 and 6.3 for the two fuel mixes and becomes:

For 85% HTPB 15% Paraffin
$$0.843(1.956G_o^{0.265}) + 0.157(2.039G_o^{-0.11}) = \dot{r}_{total} \tag{6.2}$$

(6.3)

For 70% HTPB 30% Paraffin
$$0.688(1.956G_o^{0.265}) + 0.312(2.039G_o^{-0.11}) = \dot{r}_{total} \tag{6.4}$$

(6.5)

When the equations are plotted in Fig. VI-12 for the average oxidizer mass fluxes seen, it becomes apparent that the uncertainty in the regression rate for paraffin badly affects the predicted trends for the mixed fuel.

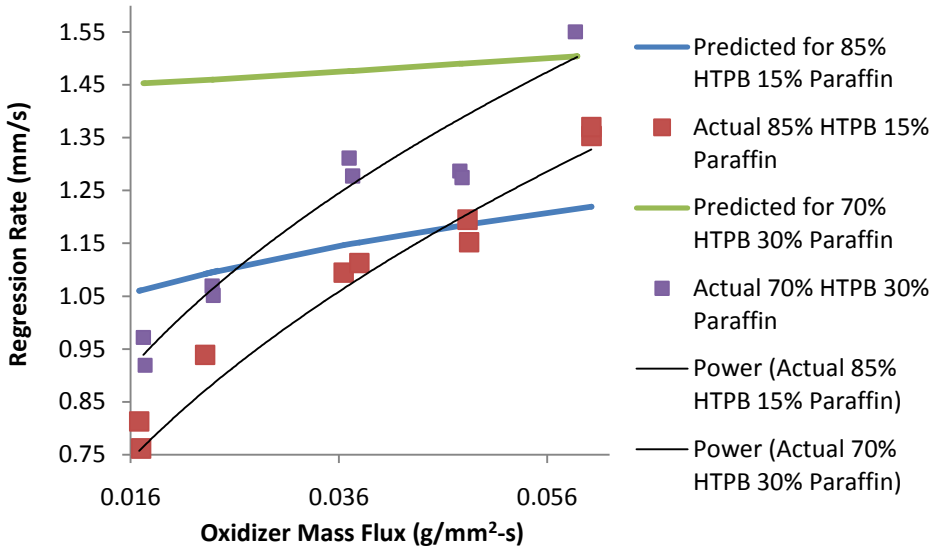

Fig. VI-12 Predicted regression rates vs actual for mix fuels

E. FURTHER DATA ANALYSIS

Since it is clear that the regression data for paraffin is not representative of a stable burn and does not enable viable regression data, further analysis was warranted. The last two data points in the paraffin data were considered better results than the first two because they did not blow out and burned until the fuel was nearly depleted. A possible improvement would be to throw out the first two paraffin data points and only include the second two. Basing a regression curve off of two points is less than ideal, but did improve the results considerably.

A replacement of Fig. VI-6 with a new Fig. VI-13 shows the regression summary with the uncertainty in the low oxidizer mass flux tests removed.

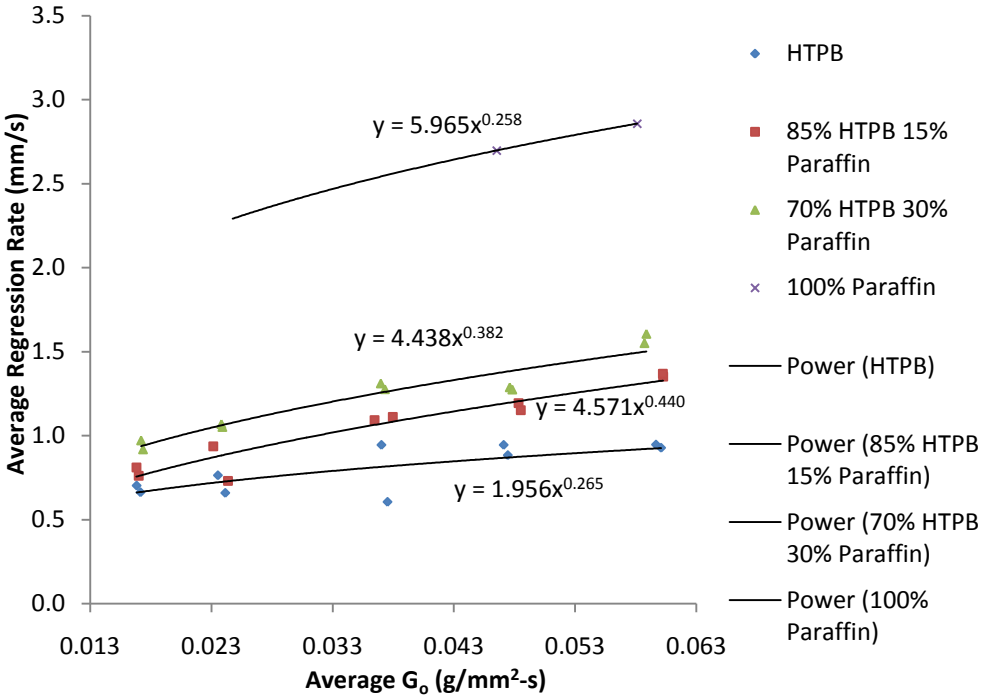

Fig. VI-13 New paraffin regression data vs average oxidizer mass flux for all fuels

The regression curve for paraffin with this plot is much more representative of paraffin regression plots in literature. The new regression equations are listed on the chart and are fit from the data using a power function. If these new equations are inserted into equation 6.1 (using the same weighting factors) a new plot of the predicted regression rate for the mixed fuels vs the actual can be made. This plot is shown in Fig. VI-14.

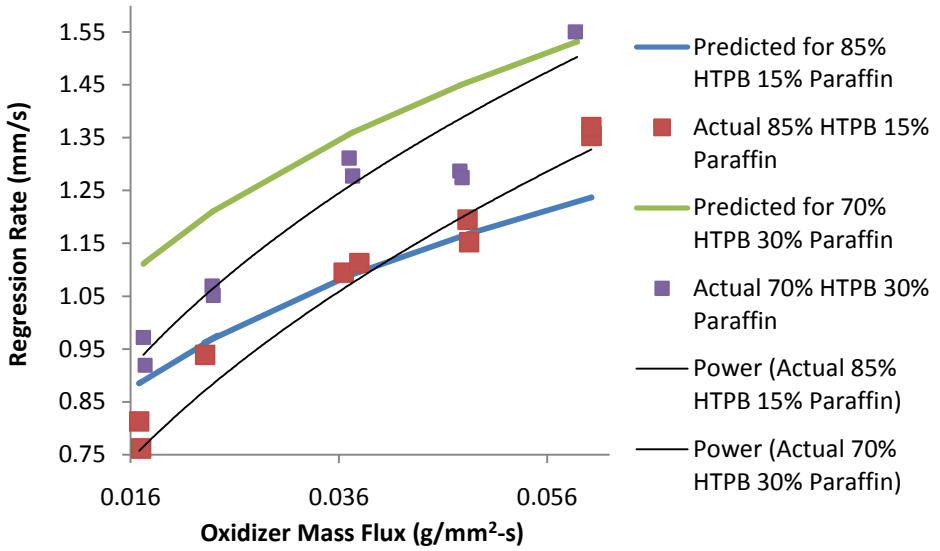

Fig. VI-14 New regression predictions vs actual results

With this new data analysis, the predictions are much closer to the actual measured data. The curves however exhibit differences between the measured and calculated values. It is possible that either the new data analysis is not enough or that equation 6.1 is not a suitable estimate for the mixed fuel regression rates at these small scales. If the latter is true, it is likely because equation 6.1 fails to account for some physical aspects that play a larger role in the real physics or scaling of very small motors.

VII. CONCLUSION AND RECOMMENDATIONS

From the results obtained, it is clear that uncertainty due to the scale of this motor played a large role in the quality of data and call into question the main results of this investigation regarding paraffin regression rates. The non-homogeneous combination fuels do significantly increase the average regression rate when compared to standard HTPB. While the trends have some uncertainty issues, they appear to show a strong benefit from the paraffin chunks that were added. The percent quantity of the respective fuels can be used via the hypothesized equation 2.17 to roughly model the improvements in regression rate, but do not precisely predict the trends at the current scale and with current data. More work is needed to refine equation 2.17 to take into account actual physical effects and develop a real theory for regression. Special attention will need to be paid to the scale of the motor when developing this theory.

Better results for the paraffin fuel tests are needed to further validate this work and to help with writing a better theory of regression for this fuel. The amount of usable data that was acquired for this test was inadequate and data had to be discarded to allow the results to compare with trends in literature. More tests in general would be required in modeling this problem. Specifically, tests at higher O/F ratios will be needed if the motor scale is kept constant. What would be more beneficial would be if the scale of the motor was increased to reduce the amount of uncertainty. One conclusion that can be drawn from this experiment is that pure paraffin cores are not well suited to a motor of this small scale utilizing oxidizer mass fluxes a system like this can deliver. Higher pressure

regulators would be able to deliver higher oxidizer rates and could perhaps solve this issue.

To expand upon this work in the future, non-homogeneous fuel combinations such as this need to be tested further and at larger scales. It would be beneficial to determine the impact of paraffin chunk size on the overall regression. A series of tests could be conducted testing varying sizes of chunks. Also, more percent quantities could be investigated to determine the full spectrum of performance from paraffin / HTPB mixes. Structural testing of the fuel would also be beneficial to directly quantify if the new mixed fuel is indeed better suited for certain applications over plain paraffin. Finally, design examples should be investigated using this new data to determine if single core non-homogeneous fuels can deliver the performance needed for applications such as sounding rocket sustainers and other such missions of interest.

REFERENCES

[1] Arves, J et all, "Overview of hybrid sounding rocket program" *33rd Joint Propulsion Conference*, AIAA, Seattle, WA 1997.

[2] Arves, J et all, "Overview of the Hybrid Sounding Rocket (HYSR) Project" *39th AIAA/ASME/SAE/ASEE Joint Propulsion Conference and Exhibit*, AIAA, Huntsville AL, 2003.

[3] Beeson, H et all, *Safe Use of Oxygen and Oxygen Systems: Handbook for Design, Operations and Maintenance*, 2nd edition ASTM MNL36-2nd. ASTM International West Conshohocken, PA. 2007.

[4] Casalino, L et all, "A Parametric Analysis of Hybrid Rocket Motors for Sounding Rockets" *44th AIAA/ASME/SAE/ASEE Joint Propulsion Conference and Exhibit*, AIAA, Hartford, CT, 2008.

[5] Chiaverini, M. Kuo, K., *Fundamentals of Hybrid Rocket Combustion and Propulsion*, Progress in Astronautics and Aeronautics, AIAA, Reston, VA. 2007.

[6] Dyer, J. et all, "Design and Development of a 100km Nitrous Oxide / Paraffin Hybrid Rocket Vehicle" *43rd AIAA/ASME/SAE/ASEE Joint Propulsion Conference and Exhibit*, AIAA, Cincinnati, OH, 2007.

[7] Dyer, J. et all, "Status Update Report for the Peregrine Sounding Rocket Project: Part III" *45th AIAA/ASME/SAE/ASEE Joint Propulsion Conference and Exhibit*, AIAA, Denver, CO, 2009.

[8] Karabeyoglu, A. et all, "Development and Testing of Paraffin-Based Hybrid Rocket Fuels" *37th AIAA/ASME/SAE/ASEE Joint Propulsion Conference and Exhibit*, AIAA, Salt Lake City, UT, 2001.

[9] Karabeyoglu, A. et all, "Scale-Up Tests of High Regression Rate Liquefying Hybrid Rocket Fuels" *Journal of Propulsion and Power Vol 20, No. 6, November - December 2004*.

[10] Karabeyoglu, A., "Mixtures of Nitrous Oxide and Oxygen (Nytrox) as Oxidizers for Rocket Propulsion Applications" *45th AIAA/ASME/SAE/ASEE Joint Propulsion Conference and Exhibit*, AIAA, Denver, CO, 2009.

[11] Kearney, D. et all, “Improvements to the Marketability of Hybrid Propulsion Technologies” *AIAA Space 2004 Conference & Exposition*, AIAA, San Diego, CA, 2004.

[12] Sutton, G. Biblarz, O., *Rocket Propulsion Elements*, 7th ed., Wiley Interscience Publication. New York, NY. 2001.

[13] Zilliac G. Karabeyoglu, A., "Hybrid Rocket Fuel Regression Rate Data Modeling" *42nd AIAA/ASME/SAE/ASEE Joint Propulsion Conference & Exhibit*, AIAA, Sacramento, CA, 2006.